Togliatto G; Trombetta A; Dentelli P; Gallo S; Rosso A; Cotogni P; Granata R; Falcioni R; Delale T; Ghigo E; Brizzi MF. Unacylated ghrelin (UnAG) induces oxidative stress resistance in a glucose intolerance mouse model and peripheral artery disease by restoring endothelial cell miR-126 expression.. DIABETES. 64 pp: 1370-1382.
DOI: 10.2337/db14-0991

Unacylated Ghrelin Induces Oxidative Stress Resistance in a Glucose Intolerance and Peripheral Artery Disease Mouse Model by Restoring Endothelial Cell miR-126 Expression

Gabriele Togliatto[1], Antonella Trombetta[1], Patrizia Dentelli[1], Sara Gallo[1], Arturo Rosso[1], Paolo Cotogni[2], Riccarda Granata[1], Rita Falcioni[3], Thomas Delale[4], Ezio Ghigo[1] and Maria Felice Brizzi[1]

1 Department of Medical Sciences, University of Turin, Turin, Italy

2 Department of Anesthesiology and Intensive Care, University of Turin, Turin, Italy

3 Department of Experimental Oncology, Regina Elena National Cancer Institute, Rome, Italy

4 Alizé Pharma, Ecully, France

Corresponding authors: Maria Felice Brizzi, mariafelice.brizzi@unito.it, and Rita Falcioni, falcioni@ifo.it.

Abstract

Reactive oxygen species (ROS) are crucial in long-term diabetes complications, including peripheral artery disease (PAD). In this study, we have investigated the potential clinical impact of unacylated ghrelin (UnAG) in a glucose intolerance and PAD mouse model. We demonstrate that UnAG is able to protect skeletal muscle and endothelial cells (ECs) from ROS imbalance in hind limb ischemia–subjected ob/ob mice. This effect translates into reductions in hind limb functional impairment. We show that UnAG rescues sirtuin 1 (SIRT1) activity and superoxide dismutase-2 (SOD-2) expression in ECs. This leads to SIRT1-mediated p53 and histone 3 lysate 56 deacetylation and results in reduced EC senescence in vivo. We demonstrate, using small interfering RNA technology, that SIRT1 is also crucial for SOD-2 expression. UnAG also renews micro-RNA (miR)-126 expression, resulting in the posttranscriptional regulation of vascular cell adhesion molecule 1 expression and a reduced number of infiltrating inflammatory cells in vivo. Loss-of-function experiments that target miR-126 demonstrate that miR-126 also controls SIRT1 and SOD-2 expression, thus confirming its role in driving UnAG-mediated EC protection against ROS imbalance. These results indicate that UnAG protects vessels from ROS imbalance in ob/ob mice by rescuing miR-126 expression, thus emphasizing its potential clinical impact in avoiding limb loss in PAD.

Introduction

Peripheral arterial disease (PAD) is a widespread condition caused by the atherosclerosis of peripheral arteries, most commonly in the lower extremities (1). Patients with both type 1 and type 2 diabetes display an increased risk of developing PAD (2,3). Moreover, individuals with diabetes develop PAD at an early age, and greater PAD severity is commonly caused by impaired vascular remodeling (2,3). The persistence of an oxidative environment is crucial for symptom occurrence/recurrence in the diabetic setting (3). A defective mitochondrial electron transport chain (4), along with an increase in reactive oxygen species (ROS) levels, are crucial determinants of tissue damage in PAD patients. This is particularly true in diabetes, in which endogenous antioxidant defense mechanisms are also impaired (3,5).

The role of glucose-mediated oxidative stress in vascular damage has been extensively documented and is considered to be the most relevant mechanism in what is known as metabolic memory (6–8). Metabolic memory refers to the long-term detrimental effects of hyperglycemia, maintained even after glucose normalization. It mainly relies on changes in the epigenome (6–8) and involves histone-modifying enzymes, DNA methylation, chromatin remodeling proteins, and micro-RNAs (miRs) (6–8). Proof of concept for the role of impaired ROS clearance in hyperglycemia-induced changes in the epigenome (9) can be found in the molecular approach-driven overexpression of superoxide dismutase-2 (SOD-2), the primary enzymatic antioxidant defense against ROS production, which prevents the sugar-induced histone methylation of the NF-κB subunit p65 (9). The transcriptional activation of NF-κB and the expression of its target genes, such as the vascular cell adhesion molecule 1 (VCAM-1), are some of the most relevant markers of epigenome modification in diabetes (9). In addition to the role of transcription factor NF-κB, posttranscriptional regulation, involving small noncoding miRs, is known to control VCAM-1 expression and inflammatory cell recruitment in developing atherosclerotic lesions and

subsequent ischemia (10). Interestingly, the plasma miR profile of diabetic patients has revealed that miR-126, one of miRs involved in the regulation of VCAM-1 expression (11), is reduced (12). This suggests that aberrant miR-126 regulation might also contribute to the long-lasting detrimental vascular effects of hyperglycemia. Persistent downregulation of class III histone deacetylase sirtuin 1 (SIRT1) (13), in individuals suffering from diabetes has also recently been reported to contribute to mitochondrial superoxide accumulation, reduced scavenging enzyme activity, NF-κB activation, p53 and histone 3 lysate 56 (H3K56) acetylation, as well as vascular dysfunction (8,13,14).

Surgical and endovascular treatment are currently considered to be the front line in avoiding limb loss (15). However, restenosis is commonly found in up to 50% of patients with successful angioplasty (16). Moreover, alternative treatment options are still limited for PAD patients who are not eligible for surgery. Therapeutic angiogenesis has recently been proposed for these patients, but has failed to improve long-term patient outcomes (2). The failure to obtain a clinical response to current therapeutic options has spurred the development of alternative strategies, which are mainly focused on improving antioxidant machinery. We have previously shown that the more abundant circulating form of ghrelin, unacylated grelin (UnAG), exerts antioxidant effects on endothelial progenitor cells (EPCs) (17,18). A proof of concept is provided by UnAG administration, which induces SOD-2 expression and improves mitochondrial dysfunction in muscles subjected to ischemia (19). UnAG is one of the ghrelin forms that is mainly produced in the stomach (20). UnAG differs from acylated ghrelin (AG) in term of its biological activity (17–19,21). Moreover, while both AG and UnAG are released into circulation (22), their ratio (AG/UnAG) varies and ranges from 1:2 to 1:9 (23), while a relative excess of AG has interestingly been found in individuals suffering from insulin resistance–connoted metabolic disorders (24). These observations, coupled with the role of glucose-mediated oxidative stress in vascular damage, have led us to investigate the clinical

impact of UnAG administration on a mouse model of massive obesity, glucose intolerance, and PAD.

Research Design and Methods

Reagents

A detailed list of the reagents and antibodies used in this study is reported in Supplementary Table 1.

Murine Hind Limb Ischemia Model

Male C57BL/6J ob/ob mice (8 weeks old) (Charles River Laboratories International Inc., Wilmington, MA) were anesthetized on day 0, and unilateral hind limb ischemia was induced as described in Hellingman et al. (25). The normoperfused contralateral limb of each mouse was used as an internal control. After hind limb ischemia, animals were treated daily with intraperitoneal injection from day 0 to day 21 using either saline or UnAG (pharmacological dose: 100 μg/kg) (19,26,27). Mice were treated according to European guidelines and policies as approved by the University of Turin Ethical Committee.

Laser Doppler Perfusion Imaging

Mice were anesthetized as above and subjected to a noninvasive assessment of ischemic limb microvascular perfusion using the laser Doppler perfusion imaging system (PIM3; Perimed) (performed at WIL Research Europe, Saint Germain-Nuelles, France). Details are reported in the Supplementary Data.

In Vivo Assessment of Limb Function

A semiquantitative estimation of foot damage (two-way ANOVA followed by the post hoc test using the Bonferroni correction for multiple comparison) was performed serially using the following classification: 3, dragging of foot (foot necrosis); 2, no dragging but no plantar flexion (foot damage); 1, plantar flexion but no toe flexion (toe damage); and 0, flexing the toes to resist gentle traction on the tail (no damage) (28).

Histological, Immunofluorescence, and Immunohistochemistry Analysis

Gastrocnemius muscles were recovered from the ischemic and normoperfused limbs of treated animals, fixed in 10% formalin, and embedded in paraffin. Tissue sections were stained with hematoxylin and eosin for histological analysis. The proportion of fibers with central nuclei (regenerating fibers) in the injured area was counted as previously described (19). Muscle sections were processed for immunofluorescence assays and immunohistochemistry analyses as previously described (29). A quantification of cells that expressed the indicated markers was obtained as previously described (30). Images were acquired using a Zeiss LSM 5 Pascal confocal laser-scanning microscope (Carl Zeiss, Jena, Germany) (19). Details are reported in the Supplementary Data.

Cell Cultures and In Vitro Ischemia

For the ex vivo experiments, endothelial cells (ECs) were isolated (31) from gastrocnemius muscles that had been subjected to ischemia. Details are reported in the Supplementary Data. For the in vitro experiments, primary ECs were either cultured for 2 days in 10% (volume for volume) bovine calf serum and basic fibroblast growth factor alone or in combination with 400 μg/mL advanced glycosylation end product (AGE) or 25 mmol/L d-glucose and either treated with UnAG (1 μmol/L) or not. At day 3, in vitro ischemia was induced as previously described (19). Satellite cells (SCs) were also isolated as described in Musarò and Barberi (32).

Senescence

Senescence was performed as previously described (33). Details are reported in the Supplementary Data.

Western Blot Analysis and Nuclear Extracts

Cells were lysed and processed as previously described (34). H3K56 acetylation was evaluated on nuclear extracts from ECs. Details are reported in the Supplementary Data.

p53 Acetylation

Cells were lysed in a cold DIM buffer supplemented with 10 μmol/L trichostatin A. Equal amounts of protein (500 μg) were immunoprecipitated using the p53 monoclonal antibody (see Supplementary Data). Bound proteins were eluted and processed as previously described (35). Immunoprecipitates were subjected to SDS-PAGE and blotted with the antiacetylated Lys382 p53 antibody.

RNA Isolation and Quantitative Real-Time PCR for miRs

Total RNA was isolated using the TRIzol reagent (Invitrogen) from ECs recovered from the muscles of treated animals or from ECs subjected to in vitro ischemia. Samples were processed as previously described (31). Loss-of-function experiments were performed in ECs transfected with an anti-miR negative control or an anti–miR-126 antagonist according to the manufacturer's instructions.

Statistical Analysis

All data are presented as mean ± SEMs. The D'Agostino-Pearson test was used to test normality. Data on blood perfusion, damage score, number of vessels, percentage of regenerating fibers, inflammatory cells, and miR-126 and VCAM-1 expression from the ischemic and nonischemic limbs of treated ob/ob mice at days 7 and 21 were analyzed using two-way ANOVA, followed by the post hoc test with the Bonferroni correction for multiple comparisons. Data on blood glucose, body weight, HbA1c measurements from adhesion assays, senescence assays, ROS generation, nitric oxide (NO) production, CD31/SOD-2 colocalization, CD31/SIRT1 colocalization, proliferating cell nuclear antigen (PCNA) expression, on glucose and insulin tolerance test assays, from luciferase assays, on miR-126 expression in in vitro or loss-of-function experiments, and SIRT1 and SOD-2 inactivation were analyzed using one-way ANOVA followed by Tukey multicomparison post hoc test. Densitometric analysis data for the Western blots were analyzed using Student t tests for

two-group comparison and one-way ANOVA, followed by Tukey's multiple comparison test, for ≥3 groups. The cutoff for statistical significance was set up at $P < 0.05$ (*$P < 0.05$, **$P < 0.01$, ***$P < 0.001$). All statistical analyses were carried out using GraphPad Prism version 5.04 (Graph Pad Software).

Blood glucose measurements, cell proliferation, FACS analyses, adhesion assays, SIRT1 and SOD-2 silencing, oxidative stress, NO detection, glucose and insulin tolerance tests, and the luciferase gene reporter are reported in the Supplementary Data.

Results

UnAG Protects ob/ob Muscles Against Hind Limb Ischemia

PAD is one of the most challenging medical-surgical diseases worldwide (1–3). The beneficial vascular effects of UnAG (17,19) have led us to investigate UnAG's therapeutic potential in ob/ob mice with PAD. ob/ob Mice that had been subjected to unilateral hind limb ischemia were treated daily (starting at day 0) with either saline or UnAG. No significant differences in large vessel reperfusion (Fig. 1A) were detected in the treatment groups as shown by laser Doppler perfusion imaging performed at the indicated number of days postsurgery. However, the functional scores reported in Fig. 1B demonstrate a significantly higher damage score in the saline- than in the UnAG-treated group. UnAG-treated ob/ob mice contained an increased number of regenerating myofibers in ischemia-subjected muscles (Fig. 1C and D), which is consistent with data obtained in wild-type mice (19). Also consistent with our previous data (19) is the finding that UnAG was able to induce an expansion in SCs (Pax-7+/MyoD+ cells) as well as their terminal differentiation (myogenin+ cells) (Fig. 1E). In order to investigate the possibility that such differences depended on UnAG-mediated vascular protection, the number of vessels in ischemic and nonischemic muscles was counted in the two groups of mice. As shown in Fig. 2A, saline-treated mice showed significantly lower capillary density in this study than in the contralateral muscles, unlike UnAG-treated animals. The expression of PCNA and cyclin D1 was then evaluated in ECs recovered from the ischemic muscles of saline and UnAG mice so as to rule out the possibility that proliferation signals may be able to mediate UnAG effects. We found that both PCNA and cyclin D1 expression were similar in the two animal groups at days 7 and 21 after surgery (PCNA: saline, day 7 = 24.09 ± 5.2; UnAG, day 7 = 20.3 ± 3.3; saline, day 21 = 20.73 ± 4.6; UnAG, day 21 = 24.5 ± 3.8; n = 3) (Fig. 2B). No changes in plasma glucose concentration (saline, 326.3 ± 28.9; UnAG, 310.1 ± 31.2 mg/dL), body weight (saline, 45.83 ± 0.76; UnAG, 45.91 ± 0.9 g), HbA1c (saline, 12.38 ± 1.09%; UnAG, 11.89

± 1.19), or insulin sensitivity (Supplementary Fig. 1A and B) were detected in UnAG mice over the entire treatment period. Thus, it can be said that UnAG protects vessels against ischemia-induced damage in ob/ob mice independently of metabolic control. In Vivo UnAG Protects Vessels Against ROS Production by Inducing SOD-2

Impaired antioxidant machinery and increased ROS production are crucial mediators of vascular damage in diabetes (36). This is particularly true in PAD patients (37), and so ECs recovered from ischemic muscles were first evaluated for intracellular ROS content. Data reported in Fig. 2C demonstrate a significant decrease in ROS generation in UnAG over saline-treated mice. In order to validate the possibility that UnAG promotes its biological effects by inducing an efficient antioxidant response, the mitochondria-specific antioxidant enzyme SOD-2 was evaluated in vessels. We demonstrate that the intramuscle vessels of UnAG-treated mice express high levels of SOD-2 (Fig. 2D). Similar results were obtained in ex vivo experiments (Fig. 2E).

UnAG Increases the Levels of SIRT1 in Ischemic Vessels and Protects ECs From Senescence

It has been reported that the impaired SIRT1 level contributes to superoxide mitochondrial accumulation in both diabetes- and insulin resistance–connoted metabolic disorders (38–40). We therefore evaluated SIRT1 expression in both saline and UnAG animals. Data reported in Fig. 3A demonstrate that UnAG treatment was associated with increased SIRT1 expression in vessels. ECs were recovered from ischemic muscles and analyzed for SIRT1 expression as a means to validate these observations. As expected, ex vivo experiments demonstrated that ECs that had been recovered from UnAG animals displayed increased SIRT1 content (Fig. 3B) both in ischemic and nonischemic muscles. Moreover, a reduced level of H3K56 acetylation (Fig. 3C) (14) and a reduced number of senescent ECs were found in ob/ob mice challenged with UnAG (Fig. 3D), which is consistent with the role of SIRT1 in regulating EC fate. SIRT1 Is Required for UnAG-Mediated EC Stress Resistance Upon Ischemia

ECs were treated with AGE and subjected to in vitro ischemia to further deepen the understanding of these data. Fig. 4A–C demonstrates that a UnAG challenge interferes with ROS generation and was able to induce both SOD-2 and SIRT1 expression. Moreover, in a finding that is consistent with our previous data in EPCs (17), we demonstrate that UnAG was able to increase NO levels in an ischemic setting (Supplementary Fig. 1C). Similar results were obtained using high glucose concentrations (data not shown). AGE was thus used throughout the study. We found that pS36p66Shc (38) was reduced in these experimental conditions, as expected from SIRT1 expression (Fig. 4D). In addition, p53 acetylation was also reduced upon UnAG treatment, and, in accordance with ex vivo experiments, this effect was associated with a reduced number of senescent ECs (Fig. 4E and F). These data were further confirmed by silencing SIRT1 (Supplementary Fig. 2A and Fig. 5A–D). Finally, UnAG treatment is only effective in reducing H3K56 acetylation in cells that express SIRT1, in vitro as well (Figs. 4G and 5E). Moreover, UnAG-induced SIRT1 activity is not enhanced by the activation of AMP-activated protein kinase (AMPK) (41), unlike calorie restriction (Fig. 4H).

It has been shown that SIRT1 activates, via its deacetylation ability, peroxisome proliferator activated receptor-γ coactivator 1α, which is involved in SOD-2 expression (42). ECs were therefore silenced for SIRT1 and subjected to the same experimental conditions. SIRT1 silencing led to reduced SOD-2 expression and increased ROS generation, even in the presence of UnAG, as shown in Fig. 5F and G. These data indicate that SIRT1 is crucial for UnAG-mediated SOD-2 expression and p53 and H3K56 deacetylation.

UnAG Hampers EC Activation and Prevents Inflammatory Cell Recruitment in Ischemic Conditions

Oxidative stress–mediated EC activation strictly controls inflammatory cell recruitment in ischemic conditions (2,3). We found that the ischemic muscles of UnAG mice had a reduced number of CD68-positive inflammatory cells (Fig. 6A). In order to investigate the possibility that UnAG

treatment protects ECs against oxidative stress–induced activation, the expression level of VCAM-1 was evaluated. Indeed, we found that vessels from UnAG animals express low levels of VCAM-1 at days 7 and 21 after ischemia when compared with control animals (Fig. 6B). Similar results were obtained both ex vivo (Fig. 6C) and in vitro when diabetes and ischemia were recapitulated (Fig. 6D and Supplementary Fig. 2B). It has been reported that molecular approaches that force SOD-2 expression led to reduced VCAM-1 expression (9,10). Thus, ECs that had been silenced for SOD-2 were evaluated (Supplementary Fig. 2C). As expected, high levels of VCAM-1 and an increased number of mononuclear cells that were adherent to ECs were detected, even in presence of UnAG (Fig. 6E and Supplementary Fig. 2D). Similar results were obtained when ECs were silenced for SIRT1 (Fig. 5H).

Posttranscriptional Mechanisms Involving miR-126 Are Crucial for UnAG Protection Against Ischemia

Besides precise transcriptional regulation, posttranscriptional regulation involving miR-126 is known to play a role in VCAM-1 expression (11). Indeed, reduced miR-126 plasma levels have been observed in diabetic patients' miR profile (12). Therefore, miR-126 levels were evaluated first on ECs recovered from ischemic muscles of UnAG- and saline-treated mice. The results shown in Fig. 7A demonstrate that the miR-126 level decreased even in ECs from saline animals. By contrast, the miR-126 level was high in ECs recovered from UnAG mice. Again, the effects of UnAG were evaluated in vitro. In accordance with the ex vivo experiments, a UnAG challenge led to miR-126 upregulation in ECs treated with AGE and subjected to ischemia (Fig. 7B, left panel). In order to gain further insight into the possibility that the posttranscriptional mechanism controls VCAM-1 expression upon UnAG treatment, the direct effect of miR-126 on VCAM-1–3′-untranslated region (UTR) was evaluated by transfecting ECs with the luciferase reporter vector containing wild-type full-length VCAM-1–3′-UTR. Increased luciferase activity was only detected in VCAM-1–3′-UTR that

expressed ECs that had been exposed to AGE and in vitro ischemia, but not when the same experiments were performed in the presence of UnAG (Fig. 7C). Furthermore, UnAG no longer had any effect on ROS production, VCAM-1 expression, or the adhesion of mononuclear cells to ECs (Fig. 7D and Supplementary Fig. 3) in loss-of-function experiments involving the transfection of ECs with anti–miR-126 antago-miRs (Fig. 7B, right panel). Interestingly, we also noticed that SOD-2 and SIRT1 content, as well as p53 and H3K56 deacetylation, were reduced by the knocking down of miR-126 (Fig. 7E–G). Furthermore, UnAG was no longer effective in protecting ECs from ROS production.

Discussion

In this study, we have shown that UnAG improves hind limb functional score in a mouse model of insulin resistance and PAD by protecting vessels against ROS-mediated damage. In particular, we have noticed that UnAG rescues ROS imbalance by restoring miR-126 expression, as well as SIRT1 and SOD-2 levels in vessels from ischemic muscles. These results indicate that restoring the AG/UnAG ratio in an insulin resistance setting can offer clinical benefits in the treatment of PAD and provide novel mechanistic insight into UnAG action.

The imbalance of two different forces, ROS and antioxidants, is crucial in long-term diabetic complications, including PAD (3,5,37). Indeed, the persistence of an oxidative milieu and the inefficient antioxidant machinery in diabetic patients with PAD also contribute to mitochondrial damage, leading to the activation of a vicious circle that clinically results in the appearance of symptoms (3,5,37). In the current study, we demonstrate that UnAG administration to mice with insulin resistance and PAD induces skeletal muscle regeneration. A resident population of adult stem cells, named SCs, is present in skeletal muscles and contributes to muscle regeneration after ischemia (43). In accordance with our previous data (19), we found that UnAG promotes SC expansion in response to ischemia. This effect results in a low damage score that, however, appears to be independent of neovascularization (PCNA and cyclin D1 content in ECs recovered from both saline and UnAG mice was similar), but arguably dependent on its antioxidant effects on ECs. As proof of concept in UnAG mice, the number of vessels in ischemic muscles was comparable to the number in nonischemic ones, and ECs recovered from ischemic muscles exhibited low levels of intracellular ROS. This suggests that UnAG, besides inducing muscle regeneration, exerts its beneficial effects in our PAD model of insulin resistance by improving the antioxidant machinery in ECs as well.

Physiologically, superoxide radicals from mitochondria are dismutated to hydrogen peroxide and oxygen by a class of enzymes called superoxide dismutases (37). Such a first line of defense against ROS mainly depends on SOD-2 (37). Human and rodent studies provide evidence for impaired SOD-2 expression in PAD muscles, particularly in patients with diabetes (37). We demonstrate in this study that SOD-2 expression is also reduced in the vessels of saline-treated mice, while it was highly expressed in vessels from UnAG-treated animals, in vivo and ex vivo. That UnAG can induce EC resistance against oxidative stress via SOD-2 is further sustained by data obtained in SOD-2–silenced ECs.

It has been reported that glucose-mediated oxidative stress and NAD+ depletion is associated with the impaired expression of SIRT1 in diabetic patient peripheral cells (40). We found that, in ob/ob mice, the SIRT1 level was lower in ECs recovered from both ischemic and nonischemic muscles of saline mice, while it increased upon a UnAG challenge. A number of SIRT1 targets have been described in mammals (44), and tumor suppressor p53 is included (38). Transcription factor p53 is involved in DNA damage mechanisms (45). However, it also acts as a negative regulator of cell proliferation in human atherosclerotic lesions (46) and contributes to accelerated vascular cell senescence in diabetes (47). We have previously reported that the silencing of p53 in EPCs from diabetic patients prevents cell senescence (47). We demonstrate in this study that UnAG-induced SIRT1 expression results in p53 deacetylation and EC protection against senescence in the ischemic condition. The pS36p66Shc level further sustains this (48).

The occurrence of vascular complications in diabetes has recently been linked to the complex interactions between genes and environmental cues that are driven by the persistence of high glucose concentrations (6–8). The impaired clearance of ROS of mitochondria origin is the most relevant environmental cue in the long-lasting detrimental effect of hyperglycemia (6–8). Growing amounts of evidence indicate that mechanisms that account for so-called “metabolic memory”

rely on the epigenetic regulation of gene expression, which can be irreversible over time (6–8). The important role that epigenetics play in long-term diabetes-associated vascular complications means that particular attention has been devoted to developing therapeutic strategies that erase epigenetics. We demonstrate in this study that, in diabetic mice subjected to ischemia, UnAG has no effect on blood glucose metabolism but interferes with some epigenetic, hyperglycemia-associated mechanisms, including histone modifying enzymes and miRs. In fact, UnAG increases SIRT1 expression by restoring miR-126 expression in ECs, which is, in turn, involved in p53 and H3K56 deacetylation and protection against DNA damage (8,13,14). Moreover, SIRT1 rescue translates into SOD-2 expression, which restores an efficient antioxidant response and further protects vessels against ROS-mediated damage. Overall, UnAG treatment recapitulates the beneficial vascular effects of SOD-2 overexpression (6,9,10). Finally, UnAG also prevents EC activation and inflammatory cell recruitment into ischemic tissues via miR-126–driven VCAM-1 posttranscriptional regulation. It has been extensively documented that the oxidant-sensitive expression of adhesion molecules is a crucial determinant of lesion progression during atherosclerosis evolution (3,5). In addition, ROS imbalance is believed to play a major role in accelerating vascular dysfunction and PAD in diabetes. Thus, UnAG might also protect vessels that are prone to atherosclerosis from undergoing lesion progression by rescuing miR-126 expression and interfering with mechanisms that control inflammatory cell homing. Finally, as NO bioavailability loss in ECs is a crucial feature of endothelial dysfunction, the increased endothelial NO detected in ECs treated with UnAG, besides controlling vascular tone, could further prevent atherogenesis and PAD progression.

We have previously shown that UnAG improves diabetic EPC mobilization by rescuing endothelial NO synthase activity in bone marrow (17). We have not analyzed EPC's contribution in the ischemic model; however, the impaired inflammatory cell recruitment observed in UnAG animals

strongly suggests that UnAG protection, rather than relying on EPC homing, may rely on their functional improvement. In accordance with this possibility is the fact that renewing miR-126 levels in diabetes rescues EPC functional capabilities and protects them against apoptosis (49). Overall, these data provide further evidence to support the theory that restoring the AG/UnAG ratio in insulin resistance–connoted pathological settings can have an impact on patients' cardiovascular risk factor profile.

The incidence of PAD, in particular, in diabetic patients is high and considered the most challenging of medical-surgical diseases (16). As current therapeutic approaches have failed to improve long-term outcomes, new therapeutic options for PAD are urgently needed. Even though an optimal treatment has yet to be identified, our results indicate that UnAG administration to ob/ob animals counteracts oxidative stress-mediated vascular dysfunction and offers clinical benefits in the treatment of PAD (Fig. 8). Although we have no direct evidence to suggest that restoring UnAG plasma concentrations in the insulin resistance state can ameliorate overall clinical outcomes, data provided in this study suggest that UnAG or UnAG-related peptides may constitute an alternative therapeutic approach to the management of one of the most relevant vascular complications in insulin resistance–connoted pathological settings. Finally, the results of this study, together with the role of mitochondrial dysfunction in the development of several metabolic and age-related disorders, suggest that exploiting UnAG-related peptides or UnAG receptor-specific agonists may also be a useful therapeutic strategy with which to address a number of currently unmet medical needs that require ROS scavenging.

Funding. This work was supported by grants from the Ministero dell'Università e della Ricerca Scientifica Progetti di Ricerca di Interesse Nazionale and Unito-Compagnia S. Paolo (to M.F.B., R.G., and E.G.), Fondazione per la Ricerca Diabetologica (FO.Ri.SID) (to M.F.B.), and Ministero della Salute (New Idea Award) and AIRC 5x1000 (SPMCO 9979) (to R.F.).

Duality of Interest. No potential conflicts of interest relevant to this article were reported.

Author Contributions. G.T. was involved in the in vivo experiments, immunoprecipitation, cell culture, and in vitro ischemia. A.T. was involved in SC isolation, histological analysis FACS, and statistical analysis. P.D. was involved in EC isolation, immunofluorescence, adhesion experiments, and luciferase assay. S.G. was involved in Western blotting, RNA isolation, and quantitative real-time PCR. A.R. was involved in construct generation and transfection. P.C. performed animal anesthesia and contributed to the implementation of the murine hind limb ischemia model. R.G. revised the manuscript. R.F. and T.D. made scientific contributions. E.G. revised the manuscript. M.F.B. was involved in study conception and design and in writing the manuscript. M.F.B. is the guarantor of this work and, as such, had full access to all the data in the study and takes responsibility for the integrity of the data and the accuracy of the data analysis.

References

1. Weitz JI, Byrne J, Clagett GP, et al. Diagnosis and treatment of chronic arterial insufficiency of the lower extremities: a critical review. Circulation 1996;94:3026–3049pmid:8941154
2. Gili M, Orsello A, Gallo S, Brizzi MF. Diabetes-associated macrovascular complications: cell-based therapy a new tool? Endocrine 2013;44:557–575pmid:23543434
3. Pitocco D, Tesauro M, Alessandro R, Ghirlanda G, Cardillo C. Oxidative stress in diabetes: implications for vascular and other complications. Int J Mol Sci 2013;14:21525–21550pmid:24177571
4. Jezek P, Hlavatá L. Mitochondria in homeostasis of reactive oxygen species in cell, tissues, and organism. Int J Biochem Cell Biol 2005;37:2478–2503pmid:16103002
5. Giacco F, Brownlee M. Oxidative stress and diabetic complications. Circ Res 2010;107:1058–1070pmid:21030723
6. El-Osta A. Glycemic memory. Curr Opin Lipidol 2012;23:24–29pmid:22186662
7. Cooper ME, El-Osta A. Epigenetics: mechanisms and implications for diabetic complications. Circ Res 2010;107:1403–1413pmid:21148447
8. Paneni F, Volpe M, Lüscher TF, Cosentino F. SIRT1, p66(Shc), and Set7/9 in vascular hyperglycemic memory: bringing all the strands together. Diabetes 2013;62:1800–1807pmid:23704521
9. El-Osta A, Brasacchio D, Yao D, et al. Transient high glucose causes persistent epigenetic changes and altered gene expression during subsequent normoglycemia. J Exp Med 2008;205:2409–2417pmid:18809715
10. Paneni F, Beckman JA, Creager MA, Cosentino F. Diabetes and vascular disease: pathophysiology, clinical consequences, and medical therapy: part I. Eur Heart J 2013;34:2436–2443pmid:23641007

11. Harris TA, Yamakuchi M, Ferlito M, Mendell JT, Lowenstein CJ. MicroRNA-126 regulates endothelial expression of vascular cell adhesion molecule 1. Proc Natl Acad Sci USA 2008;105:1516–1521pmid:18227515
12. Zampetaki A, Kiechl S, Drozdov I, et al. Plasma microRNA profiling reveals loss of endothelial miR-126 and other microRNAs in type 2 diabetes. Circ Res 2010;107:810–817pmid:20651284
13. Zhou S, Chen HZ, Wan YZ, et al. Repression of P66Shc expression by SIRT1 contributes to the prevention of hyperglycemia-induced endothelial dysfunction. Circ Res 2011;109:639–648pmid:21778425
14. Das C, Lucia MS, Hansen KC, Tyler JK. CBP/p300-mediated acetylation of histone H3 on lysine 56. Nature 2009;459:113–117pmid:19270680
15. Perera GB, Lyden SP. Current trends in lower extremity revascularization. Surg Clin North Am 2007;87:1135–1147, xpmid:17936479
16. Cieri E, Lenti M, De Rango P, Isernia G, Marucchini A, Cao P. Functional ability in patients with critical limb ischaemia is unaffected by successful revascularisation. Eur J Vasc Endovasc Surg 2011;41:256–263pmid:21130005
17. Togliatto G, Trombetta A, Dentelli P, et al. Unacylated ghrelin rescues endothelial progenitor cell function in individuals with type 2 diabetes. Diabetes 2010;59:1016–1025pmid:20068135
18. Granata R, Settanni F, Julien M, et al. Des-acyl ghrelin fragments and analogues promote survival of pancreatic β-cells and human pancreatic islets and prevent diabetes in streptozotocin-treated rats. J Med Chem 2012;55:2585–2596pmid:22352743
19. Togliatto G, Trombetta A, Dentelli P, et al. Unacylated ghrelin promotes skeletal muscle regeneration following hindlimb ischemia via SOD-2-mediated miR-221/222 expression. J Am Heart Assoc 2013;2:e000376pmid:24308935

20. Kojima M, Hosoda H, Date Y, Nakazato M, Matsuo H, Kangawa K. Ghrelin is a growth-hormone-releasing acylated peptide from stomach. Nature 1999;402:656–660pmid:10604470
21. Lear PV, Iglesias MJ, Feijóo-Bandín S, et al. Des-acyl ghrelin has specific binding sites and different metabolic effects from ghrelin in cardiomyocytes. Endocrinology 2010;151:3286–3298pmid:20410201
22. van der Lely AJ, Tschöp M, Heiman ML, Ghigo E. Biological, physiological, pathophysiological, and pharmacological aspects of ghrelin. Endocr Rev 2004;25:426–457pmid:15180951
23. Kojima M, Kangawa K. Ghrelin: structure and function. Physiol Rev 2005;85:495–522pmid:15788704
24. Barazzoni R, Zanetti M, Ferreira C, et al. Relationships between desacylated and acylated ghrelin and insulin sensitivity in the metabolic syndrome. J Clin Endocrinol Metab 2007;92:3935–3940pmid:17652221
25. Hellingman AA, Bastiaansen AJ, de Vries MR, et al. Variations in surgical procedures for hind limb ischaemia mouse models result in differences in collateral formation. Eur J Vasc Endovasc Surg 2010;40:796–803pmid:20705493
26. Nagaya N, Uematsu M, Kojima M, et al. Chronic administration of ghrelin improves left ventricular dysfunction and attenuates development of cardiac cachexia in rats with heart failure. Circulation 2001;104:1430–1435pmid:11560861
27. Porporato PE, Filigheddu N, Reano S, et al. Acylated and unacylated ghrelin impair skeletal muscle atrophy in mice. J Clin Invest 2013;123:611–622pmid:23281394
28. Bosch-Marce M, Okuyama H, Wesley JB, et al. Effects of aging and hypoxia-inducible factor-1 activity on angiogenic cell mobilization and recovery of perfusion after limb ischemia. Circ Res 2007;101:1310–1318pmid:17932327

29. Zeoli A, Dentelli P, Rosso A, et al. Interleukin-3 promotes expansion of hemopoietic-derived CD45+ angiogenic cells and their arterial commitment via STAT5 activation. Blood 2008;112:350–361pmid:18460645
30. Brizzi MF, Dentelli P, Rosso A, et al. RAGE- and TGF-beta receptor-mediated signals converge on STAT5 and p21waf to control cell-cycle progression of mesangial cells: a possible role in the development and progression of diabetic nephropathy. FASEB J 2004;18:1249–1251pmid:15180953
31. Togliatto G, Trombetta A, Dentelli P, Rosso A, Brizzi MF. MIR221/MIR222-driven post-transcriptional regulation of P27KIP1 and P57KIP2 is crucial for high-glucose- and AGE-mediated vascular cell damage. Diabetologia 2011;54:1930–1940pmid:21461636
32. Musarò A, Barberi L. Isolation and culture of mouse satellite cells. Methods Mol Biol 2010;633:101–111pmid:20204623
33. Brizzi MF, Dentelli P, Pavan M, et al. Diabetic LDL inhibits cell-cycle progression via STAT5B and p21(waf). J Clin Invest 2002;109:111–119pmid:11781356
34. Dentelli P, Trombetta A, Togliatto G, et al. Formation of STAT5/PPARgamma transcriptional complex modulates angiogenic cell bioavailability in diabetes. Arterioscler Thromb Vasc Biol 2009;29:114–120pmid:18927468
35. Uberti B, Dentelli P, Rosso A, Defilippi P, Brizzi MF. Inhibition of β1 integrin and IL-3Rβ common subunit interaction hinders tumour angiogenesis. Oncogene 2010;29:6581–6590pmid:20802515
36. Shenouda SM, Widlansky ME, Chen K, et al. Altered mitochondrial dynamics contributes to endothelial dysfunction in diabetes mellitus. Circulation 2011;124:444–453pmid:21747057
37. Pipinos II, Judge AR, Selsby JT, et al. The myopathy of peripheral arterial occlusive disease: Part 2. Oxidative stress, neuropathy, and shift in muscle fiber type. Vasc Endovascular Surg 2008;42:101–112pmid:18390972

38. Motta MC, Divecha N, Lemieux M, et al. Mammalian SIRT1 represses forkhead transcription factors. Cell 2004;116:551–563pmid:14980222
39. Horio Y, Hayashi T, Kuno A, Kunimoto R. Cellular and molecular effects of sirtuins in health and disease. Clin Sci (Lond) 2011;121:191–203pmid:21599635
40. de Kreutzenberg SV, Ceolotto G, Papparella I, et al. Downregulation of the longevity-associated protein sirtuin 1 in insulin resistance and metabolic syndrome: potential biochemical mechanisms. Diabetes 2010;59:1006–1015pmid:20068143
41. Cantó C, Gerhart-Hines Z, Feige JN, et al. AMPK regulates energy expenditure by modulating NAD+ metabolism and SIRT1 activity. Nature 2009;458:1056–1060pmid:19262508
42. Gerhart-Hines Z, Rodgers JT, Bare O, et al. Metabolic control of muscle mitochondrial function and fatty acid oxidation through SIRT1/PGC-1alpha. EMBO J 2007;26:1913–1923pmid:17347648
43. Kuang S, Gillespie MA, Rudnicki MA. Niche regulation of muscle satellite cell self-renewal and differentiation. Cell Stem Cell 2008;2:22–31pmid:18371418
44. Baur JA, Ungvari Z, Minor RK, Le Couteur DG, de Cabo R. Are sirtuins viable targets for improving healthspan and lifespan? Nat Rev Drug Discov 2012;11:443–461pmid:22653216
45. Salama R, Sadaie M, Hoare M, Narita M. Cellular senescence and its effector programs. Genes Dev 2014;28:99–114pmid:24449267
46. Mercer J, Bennett M. The role of p53 in atherosclerosis. Cell Cycle 2006;5:1907–1909pmid:16929177
47. Rosso A, Balsamo A, Gambino R, et al. p53 Mediates the accelerated onset of senescence of endothelial progenitor cells in diabetes. J Biol Chem 2006;281:4339–4347pmid:16339764
48. Pinton P, Rimessi A, Marchi S, et al. Protein kinase C beta and prolyl isomerase 1 regulate mitochondrial effects of the life-span determinant p66Shc. Science 2007;315:659–663pmid:17272725

49. Meng S, Cao JT, Zhang B, Zhou Q, Shen CX, Wang CQ. Downregulation of microRNA-126 in endothelial progenitor cells from diabetes patients, impairs their functional properties, via target gene Spred-1. J Mol Cell Cardiol 2012;53:64–72pmid:22525256

Figure Legends

Figure 1

UnAG protects ob/ob mice against ischemia-induced functional impairment. A: Histogram representation of blood perfusion reported as ratio (mean ± SEM, n = 13 for each group) of ischemic to normal hind limb for both groups of mice (0b, before surgery; 0a, after surgery). B: Foot damage score was evaluated for the indicated times. Data are expressed as mean ± SEM; n = 13. *P < 0.05 UnAG vs. saline in ischemic limb. C: Representative hematoxylin and eosin–stained sections of ischemic muscles from saline- and UnAG-treated mice, at days 7 and 21 postsurgery. Scale bars, 80 μm (×20 magnification). Insets show regenerating myofibers at higher magnification. D: Quantification of the percentage (mean ± SEM) of regenerating fibers, characterized by the presence of a centrally located nucleus. UnAG- and saline-treated mice were analyzed at days 7 and 21 postsurgery. *P < 0.05 UnAG-treated mice at day 7 vs. day 21; ***P < 0.001 ischemic muscles of UnAG- vs. saline-treated mice at days 7 and 21. E: Cell extracts from SCs recovered from ischemic muscles at days 7 and 21 were analyzed by Western blot for Pax-7, MyoD, and myogenin content and normalized to tubulin content. **P < 0.01 myogenin from UnAG-treated mice at day 7 vs. day 21; ***P < 0.001 Pax-7 and MyoD content in ischemic SCs from UnAG- vs. saline-treated mice at day 7; ***P < 0.001 myogenin content in ischemic SCs from UnAG- vs. saline-treated mice at day 21; ***P < 0.001 Pax-7 and MyoD from UnAG-treated mice at day 7 vs. day 21. A–D: n = 13 each group at days 7 and 21. E: n = 3 each group at days 7 and 21. LDPI, laser Doppler perfusion imaging

Figure 2

UnAG protects the intramuscle vessels of ob/ob mice subjected to hind limb ischemia and increases SOD-2 expression. A: Sections of ischemic muscles recovered from saline- and UnAG-treated mice at days 7 and 21 postsurgery were stained for CD31 (red) and DAPI (blue). Red

arrows indicate vessels. Scale bars, 40 μm (×40 magnification). The graph on the right represents the number of vessels in ischemic (ih) and normoperfused (nh) gastrocnemius muscles as evaluated by three different operators counting 10 fields at ×40 magnification and reported as mean ± SEM (n = 7 each group at days 7 and 21) of vessels per field. ***P < 0.001 ih muscles of UnAG mice vs. ih muscles of saline mice at days 7 and 21. B: Cell extracts of ECs recovered from ischemic muscles of treated mice at days 7 and 21 were analyzed for cyclin D1 content by Western blot and normalized to β-actin content. The results are representative of three different experiments. C: Intracellular ROS generation was analyzed using a Amplex Red fluorescence assay kit on ECs recovered from muscles of treated mice by cell-magnetic sorting at day 21 after ischemia. The fluorescence level (mean ± SEM, n = 3 each group) is reported as fold induction relative to "saline" values, which were arbitrarily set as 100. *P < 0.05 UnAG- vs. saline-treated mice. D: Representative stained sections for CD31 (red), SOD-2 (green), and DAPI (blue) of muscles recovered at days 7 and 21 postsurgery. Insets show SOD-2 and CD31 colocalization at higher magnification. Scale bars, 40 μm (×40 magnification). Quantification of SOD-2+/CD31+ cells per field (×40 magnification) in ischemic vessels of treated mice is reported in the graph at right (mean ± SEM, n = 7 each group). ***P < 0.001 UnAG- vs. saline-treated mice at days 7 and 21. E: Cell extracts of ECs recovered from ischemic muscles of treated mice at day 21 were analyzed for SOD-2 content by Western blot and normalized to β-actin content. The results are representative of three different experiments. *P < 0.05 ECs from UnAG- vs. saline-treated mice.

Figure 3

UnAG increases SIRT1 levels in ischemic vessels and protects ECs from senescence. A: Representative stained sections for CD31 (red), SIRT1 (green), and DAPI (blue) of muscles recovered at days 7 and 21 after ischemia. Insets show SIRT1 and CD31 colocalization at higher magnification. Scale bar, 40 μm (×40 magnification). Quantification of SIRT1+/CD31+ cells per field

(×40 magnification) in ischemic vessels of treated mice is reported in the graph (mean ± SEM, n = 7 each group) (***P < 0.001 UnAG- vs. saline-treated mice at days 7 and 21). B: ECs recovered from nonischemic or ischemic muscles as described in research design and methods were subjected to Western blot analysis for SIRT1 content. Protein levels were normalized to β-actin content. **P < 0.01 UnAG- vs. saline-treated mice for nonischemic ECs (top); **P < 0.01 UnAG- vs. saline-treated mice for ischemic ECs (bottom); n = 3. C: Cell extracts from ECs recovered from the ischemic muscles of treated mice were analyzed for H3K56ac content, which was normalized to H3 content. **P < 0.01 UnAG vs. saline; n = 3. D: Senescence was evaluated on ECs recovered from ischemic muscles at day 21 and expressed as the mean ± SEM of SA–β-gal–positive cells per field. **P < 0.01 UnAG vs. saline; n = 3. H3K56ac, H3K56 acetylation.

Figure 4

In vivo UnAG effects are recapitulated in ECs subjected to in vitro ischemia. A: Intracellular ROS generation was evaluated using an Amplex Red fluorescence assay kit in ECs subjected to in vitro ischemia and untreated (c) or treated with AGE (A), UnAG (U), or AGE+UnAG (A+U). Fluorescence level (mean ± SEM, n = 4) is reported as fold induction relative to control values, which were arbitrarily set as 100. **P < 0.01 AGE-treated vs. untreated ECs; ***P < 0.001 UnAG-treated and AGE+UnAG vs. AGE-treated ECs. Cell extracts from ECs subjected to in vitro ischemia and treated as indicated were analyzed for SIRT1 (B), SOD-2 (C), and pS36p66Shc (p-p66Shc) (D) content, normalized to β-actin and p66Shc content, or for acetylated and total p53 content (E). *P < 0.05 for p-p66Shc UnAG and AGE+UnAG vs. untreated or AGE-treated ECs; **P < 0.01 for SIRT1, ***P < 0.001 for SOD-2 (C), ***P < 0.001 for acetylated p53 in UnAG and AGE+UnAG vs. AGE (E). F: Senescence was evaluated on ECs treated as above and expressed as the mean ± SEM of SA–β-gal–positive cells per field. ***P < 0.001 UnAG and AGE+UnAG vs. untreated or AGE. Empty bar, control (ctrl); diagonal line bar, AGE; horizontal line bar, UnAG; and black bar, UnAG+AGE. Nuclear

H3K56ac (G) and cytoplasmatic phospho-(p)-AMPK (H) content was evaluated in ECs treated as indicated. Protein levels were normalized to H3 or AMPK content, respectively. ***P < 0.001 AGE vs. untreated and UnAG or AGE+UnAG vs. AGE for H3K56ac. All results are representative of four different experiments performed in triplicate. H3K56ac, H3K56 acetylation; IB, immunoblot; IP, immunoprecipitation.

Figure 5

SIRT1 is required for UnAG-mediated stress resistance upon ischemia. A–C: ECs that were untreated (c) or treated with AGE (A), UnAG (U), or AGE+UnAG (A+U) were transfected for 48 h with SIRT1 small interfering RNA (siRNA) and subjected to in vitro ischemia. Western blot analysis was performed to evaluate the content of SIRT1 (A) and pS36p66Shc (p-p66Shc) (B), normalized to β-actin and p66Shc content and acetylated or total p53 content (C). D: Senescence was evaluated on ECs treated as above and expressed as the mean ± SEM of SA–β-gal–positive cells per field. Empty bar, control (ctrl); diagonal line bar, AGE; horizontal line bar, UnAG; and black bar, UnAG+AGE. Cell extracts from ECs treated as above were subjected to Western blot analysis to evaluate H3K56ac and H3 content (E) or SOD-2, VCAM-1, and β-actin content (F). G: Intracellular ROS generation was evaluated using the Amplex Red fluorescence assay kit in ECs treated as indicated and subjected to in vitro ischemia. Fluorescence level (mean ± SEM, n = 4) is reported as fold induction relative to control values, which were arbitrarily set as 100. H: The adhesion assay was performed by plating red-labeled peripheral blood mononuclear cells on an EC monolayer that had previously been silenced for SIRT1. Treatments are indicated. Adherent cells were counted and reported as mean ± SEM per field (×20 magnification). All results are representative of four different experiments performed in triplicate. H3K56ac, H3K56 acetylation; IB, immunoblot; IP, immunoprecipitation.

Figure 6

UnAG hampers EC activation and prevents inflammatory cell recruitment in ischemic conditions. A: Sections of ischemic muscle that had been recovered from saline- and UnAG-treated mice, 7 and 21 days postsurgery, and stained for CD68 (red) and DAPI (blue). Scale bars, 40 μm (×40 magnification). Quantification of inflammatory cells in the ischemic muscles from treated mice at indicated times is reported. Data are expressed as mean ± SEM (n = 7 each group at day 7 and day 21) of CD68+ cells per field (×40 magnification). ***P < 0.001 ischemic muscles of saline- vs. UnAG-treated mice at days 7 and 21. B: Representative sections of VCAM-1 expression in the ECs of muscles recovered at days 7 and 21 postsurgery from saline- and UnAG-treated mice. Immunohistochemistry analyses are reported. Scale bars, 40 μm (×40 magnification). Quantification of VCAM-1+ cells per field (×40 magnification) in ischemic vessels of treated mice is reported in the graph (mean ± SEM, n = 7 each group). ***P < 0.001 UnAG- vs. saline-treated mice at days 7 and 21. C: ECs recovered from ischemic muscles at day 21 were subjected to Western blot analysis for VCAM-1 content. Protein levels were normalized to β-actin content. *P < 0.05 UnAG- vs. saline-treated mice; n = 3. D: Cell extracts from ECs subjected to in vitro ischemia and treated as indicated were evaluated for VCAM-1 and β-actin content. *P < 0.05 AGE+UnAG vs. AGE; ***P < 0.001 AGE vs. untreated cells. E: ECs untreated (c) or treated with AGE (A), UnAG (U), or AGE+UnAG (A+U) were transfected for 48 h with small interfering RNA (siRNA) of SOD-2 and subjected to in vitro ischemia. Western blot analysis was performed to evaluate the content of SOD-2 and VCAM-1, normalized to β-actin content. The results in D and E are representative of four different experiments performed in triplicate.

Figure 7

miR-126 is crucial for UnAG-mediated vessel protection against ischemia. A: miR-126 expression was evaluated by quantitative real-time PCR on ECs recovered from the ischemic muscles of mice

treated as indicated at days 7 and 21 postsurgery. Data normalized to RNU6B are representative of three experiments (n = 3 each group). ***P < 0.001 UnAG- vs. saline-treated mice at days 7 and 21. B: miR-126 expression was evaluated by quantitative real-time PCR in two groups of ECs that had either undergone transfection with anti–miR-126 oligonucleotides or not were treated with the indicated stimuli and subjected to in vitro ischemia. Data normalized to RNU6B are representative of four experiments. **P < 0.01 AGE+UnAG vs. AGE (left); **P < 0.01 treated vs. untreated ECs transfected with anti–miR-126 (right); ***P < 0.001 UnAG vs. untreated cells. C: ECs were either transfected with pGL3 empty vector or pGL3–3′-UTR full-length–VCAM-1 luciferase constructs, treated as indicated, and subjected to in vitro ischemia. Relative luciferase activity is reported. ***P < 0.001 AGE vs. untreated cells and AGE+UnAG vs. AGE; n = 4. Empty bar, control (c); diagonal line bar, AGE (A); horizontal line bar, UnAG (U); and black bar, UnAG+AGE (A+U). Cell extracts from ECs transfected with anti–miR-126 and treated as above were analyzed for VCAM-1 (D), SIRT1 and SOD-2 (E), and H3K56ac (F) content, normalized to β-actin or H3 content, as indicated, or for acetylated and total p53 content (G). The results in D–G are representative of four different experiments performed in triplicate. ctrl, control; H3K56ac, H3K56 acetylation; IB, immunoblot; IP, immunoprecipitation.

Figure 8

Schematic representation of UnAG effects following ischemia. Following muscle damage, UnAG induces skeletal muscle regeneration via SC proliferation and differentiation and vascular cell protection. Its effects are mediated by miR-126 upregulation. The increased level of miR-126 leads to: a) increased SIRT1 expression, which prevents cell senescence via epigenetic mechanisms (reduced p53 and H3K56 acetylation); b) increased SOD-2 expression, which protects ECs from ROS generation and, in turn, contributes to avoiding cell senescence; and c) reduced

VCAM-1 expression and inflammatory cell recruitment. H3K56ac, H3K56 acetylation; p53ac, acetylated p53.

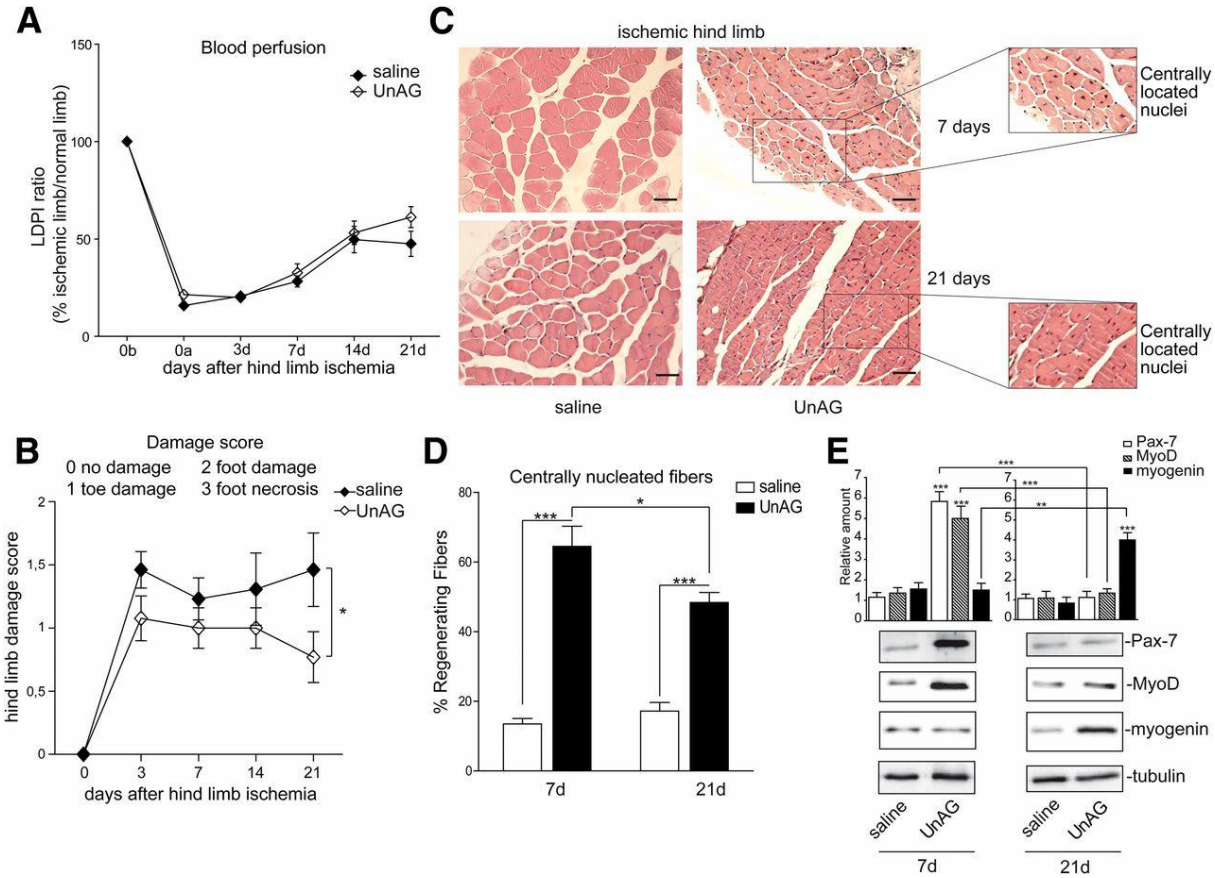
A
Blood perfusion
saline
UnAG
LDPI ratio
(% ischemic limb/normal limb)
150
100
50
0
0b
0a
3d
7d
14d
21d
days after hind limb ischemia
C
ischemic hind limb
7 days
21 days
Centrally
located
nuclei
Centrally
located
nuclei
saline
UnAG
B
Damage score
0 no damage
1 toe damage
2 foot damage
3 foot necrosis
saline
UnAG
hind limb damage score
2
1,5
1
0,5
0
0
3
7
14
21
days after hind limb ischemia
*
D
Centrally nucleated fibers
saline
UnAG
% Regenerating Fibers
80
60
40
20
0
***
*
***
7d
21d
E
Pax-7
MyoD
myogenin
Relative amount
7
6
5
4
3
2
1
0
***
***
***
***
**
***
-Pax-7
-MyoD
-myogenin
-tubulin
saline
UnAG
saline
UnAG
7d
21d

Figure 1

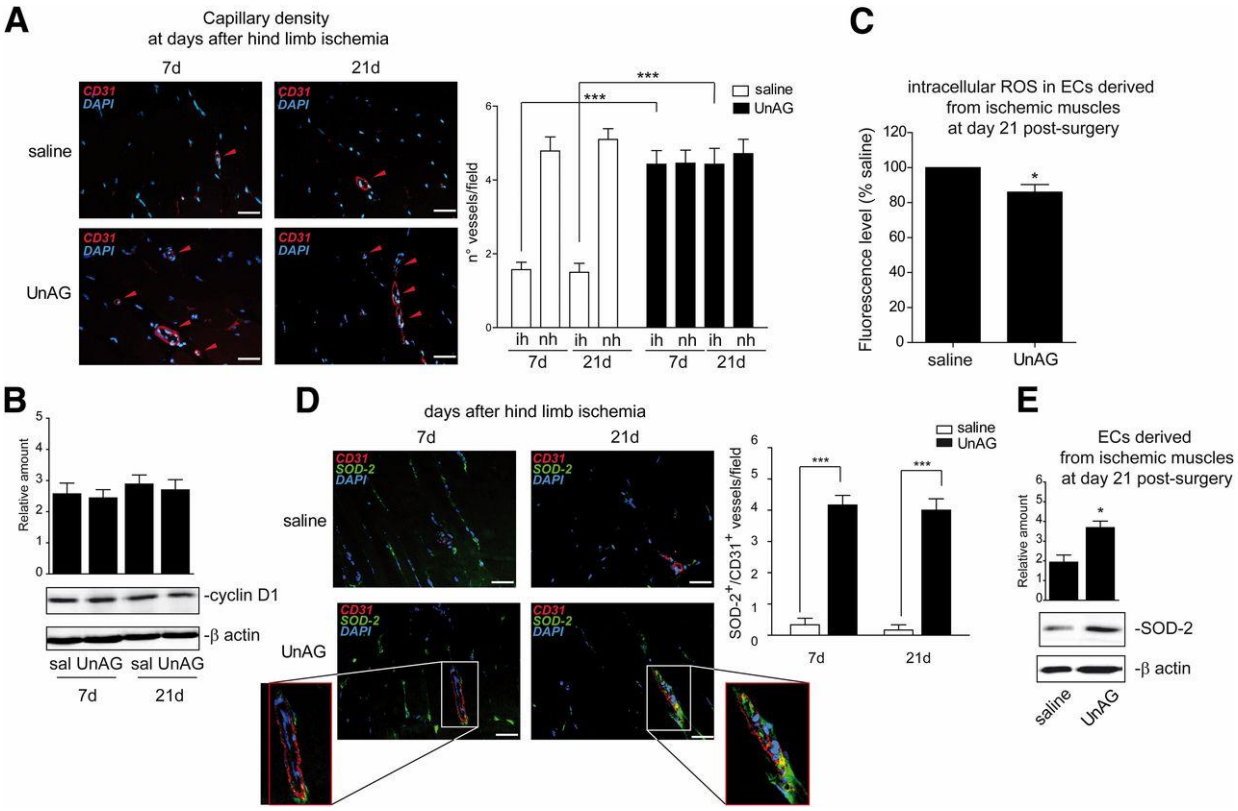
A
Capillary density
at days after hind limb ischemia
7d
21d
saline
UnAG
CD31
DAPI
n° vessels/field
saline
UnAG
ih nh ih nh ih nh ih nh
7d 21d 7d 21d
C
intracellular ROS in ECs derived
from ischemic muscles
at day 21 post-surgery
Fluorescence level (% saline)
saline
UnAG
B
Relative amount
-cyclin D1
-β actin
sal UnAG sal UnAG
7d 21d
D
days after hind limb ischemia
7d
21d
saline
UnAG
CD31
SOD-2
DAPI
SOD-2+/CD31+ vessels/field
E
ECs derived
from ischemic muscles
at day 21 post-surgery
Relative amount
-SOD-2
-β actin
saline
UnAG

Figure 2

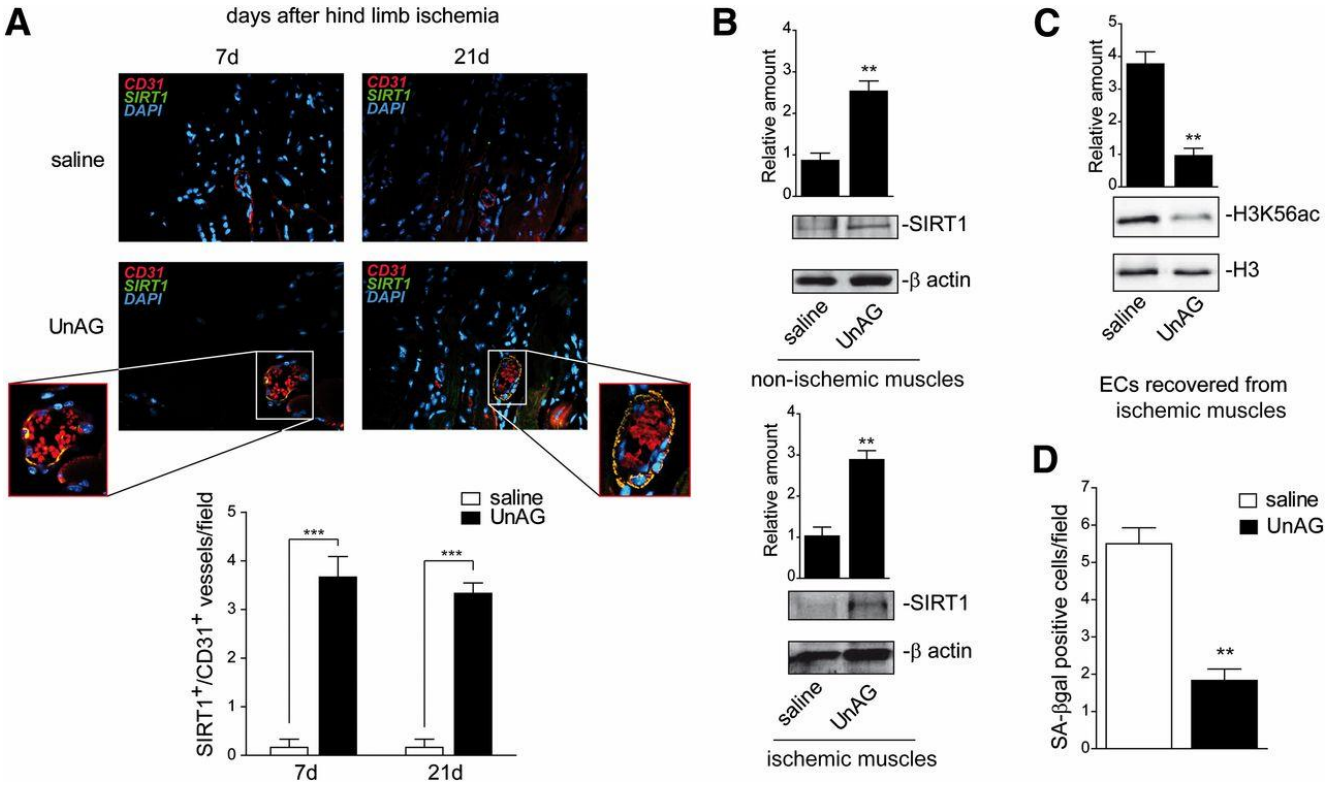
A
days after hind limb ischemia
7d
21d
saline
UnAG
CD31
SIRT1
DAPI
SIRT1+/CD31+ vessels/field
saline
UnAG
***
7d
21d
B
Relative amount
**
-SIRT1
-β actin
saline
UnAG
non-ischemic muscles
ischemic muscles
C
Relative amount
-H3K56ac
-H3
ECs recovered from ischemic muscles
D
SA-βgal positive cells/field

Figure 3

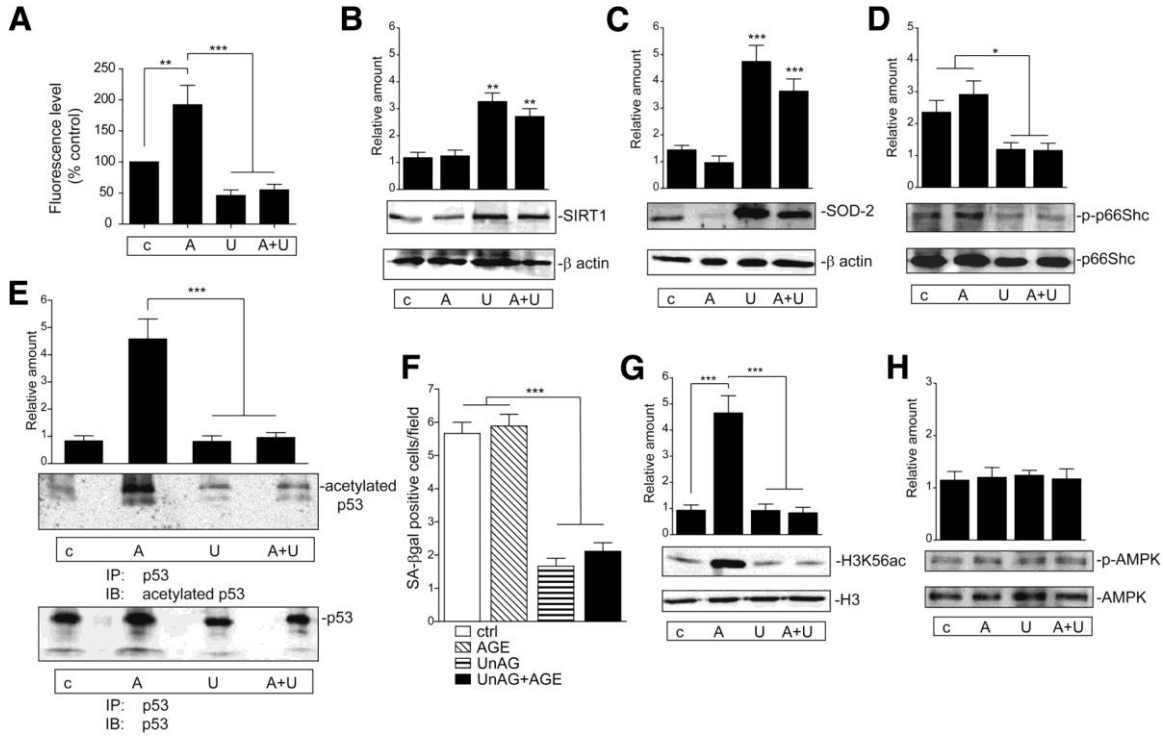
A
Fluorescence level (% control)
c A U A+U
B
Relative amount
-SIRT1
-β actin
C
-SOD-2
-β actin
D
-p-p66Shc
-p66Shc
E
-acetylated p53
IP: p53
IB: acetylated p53
-p53
IP: p53
IB: p53
F
SA-βgal positive cells/field
ctrl
AGE
UnAG
UnAG+AGE
G
-H3K56ac
-H3
H
-p-AMPK
-AMPK

Figure 4

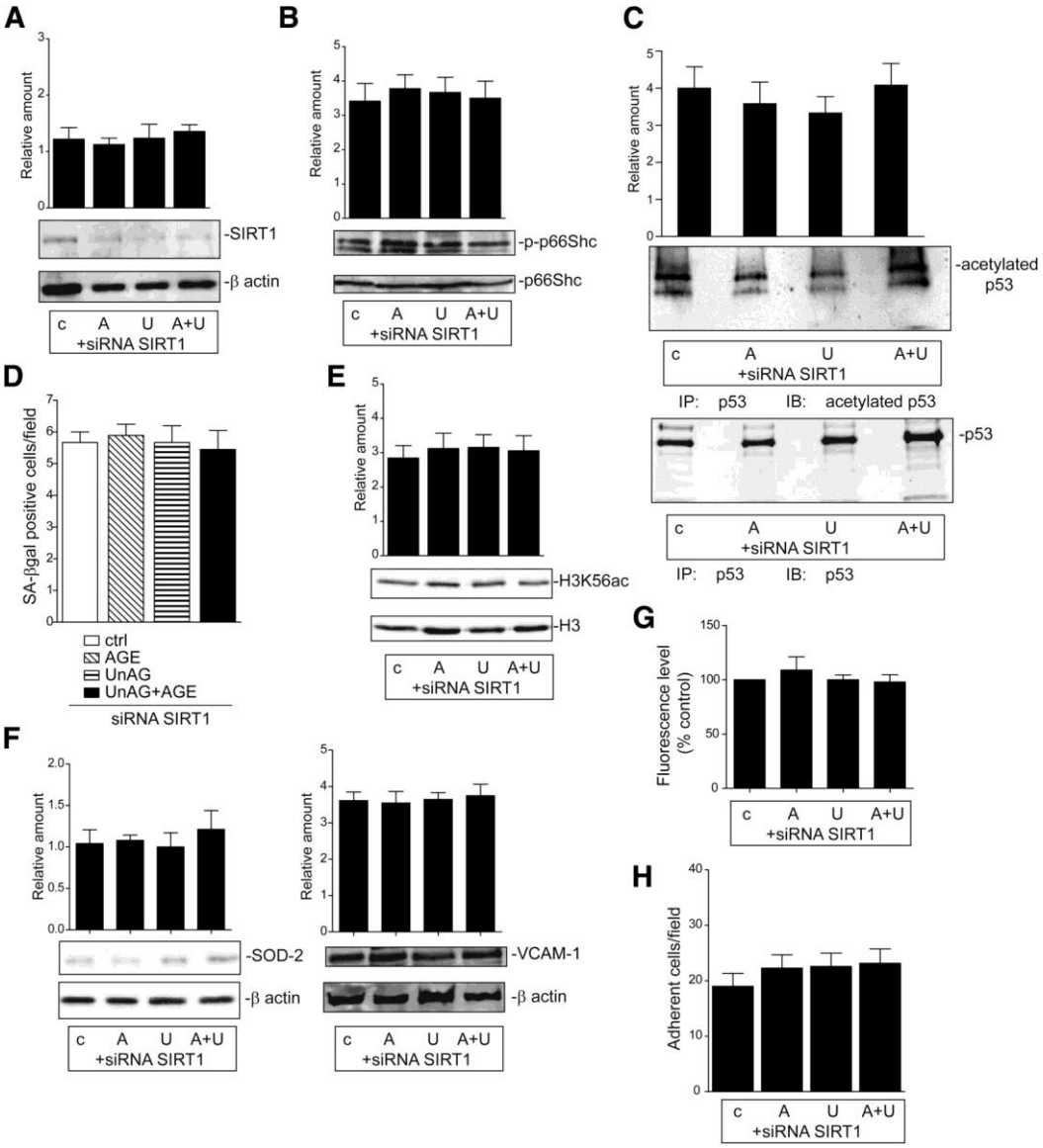
A
Relative amount
-SIRT1
-β actin
c A U A+U
+siRNA SIRT1
B
Relative amount
-p-p66Shc
-p66Shc
c A U A+U
+siRNA SIRT1
C
Relative amount
-acetylated p53
c A U A+U
+siRNA SIRT1
IP: p53 IB: acetylated p53
-p53
c A U A+U
+siRNA SIRT1
IP: p53 IB: p53
D
SA-βgal positive cells/field
ctrl
AGE
UnAG
UnAG+AGE
siRNA SIRT1
E
Relative amount
-H3K56ac
-H3
c A U A+U
+siRNA SIRT1
F
Relative amount
-SOD-2
-β actin
c A U A+U
+siRNA SIRT1
Relative amount
-VCAM-1
-β actin
c A U A+U
+siRNA SIRT1
G
Fluorescence level (% control)
c A U A+U
+siRNA SIRT1
H
Adherent cells/field
c A U A+U
+siRNA SIRT1

Figure 5

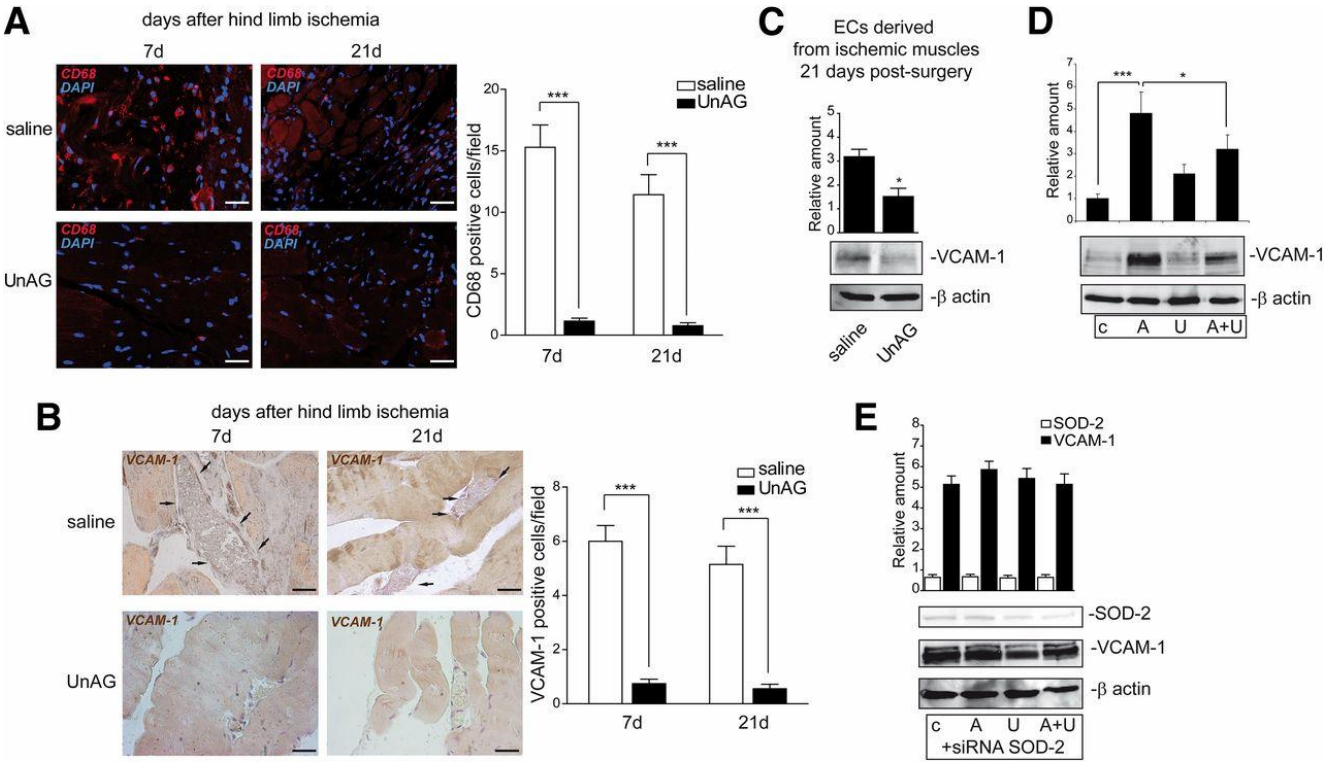
A
days after hind limb ischemia
7d
21d
saline
UnAG
CD68
DAPI
CD68 positive cells/field
saline
UnAG
***
7d
21d
C
ECs derived
from ischemic muscles
21 days post-surgery
Relative amount
-VCAM-1
-β actin
saline
UnAG
D
Relative amount
-VCAM-1
-β actin
c A U A+U
B
days after hind limb ischemia
7d
21d
saline
UnAG
VCAM-1
VCAM-1 positive cells/field
E
SOD-2
VCAM-1
Relative amount
-SOD-2
-VCAM-1
-β actin
c A U A+U
+siRNA SOD-2

Figure 6

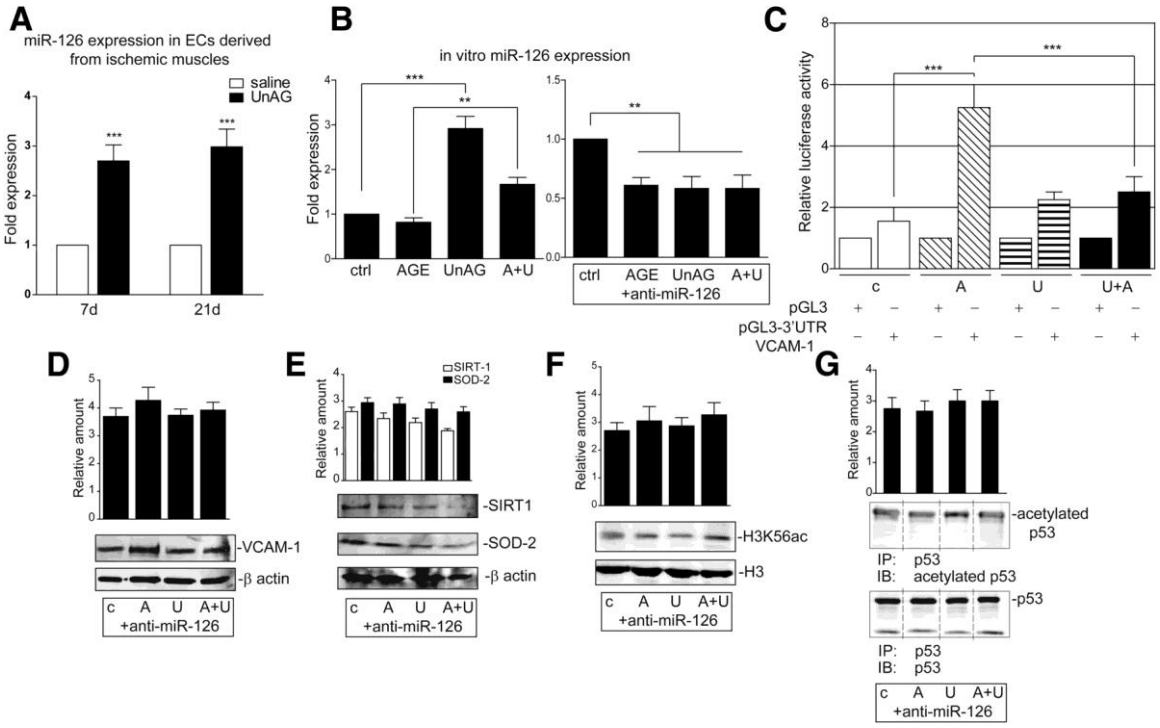
A
miR-126 expression in ECs derived from ischemic muscles
saline
UnAG
Fold expression
7d
21d
B
in vitro miR-126 expression
Fold expression
ctrl
AGE
UnAG
A+U
+anti-miR-126
C
Relative luciferase activity
c
A
U
U+A
pGL3
pGL3-3'UTR
VCAM-1
D
Relative amount
-VCAM-1
-β actin
+anti-miR-126
E
SIRT-1
SOD-2
-SIRT1
-SOD-2
-β actin
+anti-miR-126
F
Relative amount
-H3K56ac
-H3
+anti-miR-126
G
Relative amount
-acetylated p53
IP: p53
IB: acetylated p53
-p53
IP: p53
IB: p53
+anti-miR-126

Figure 7

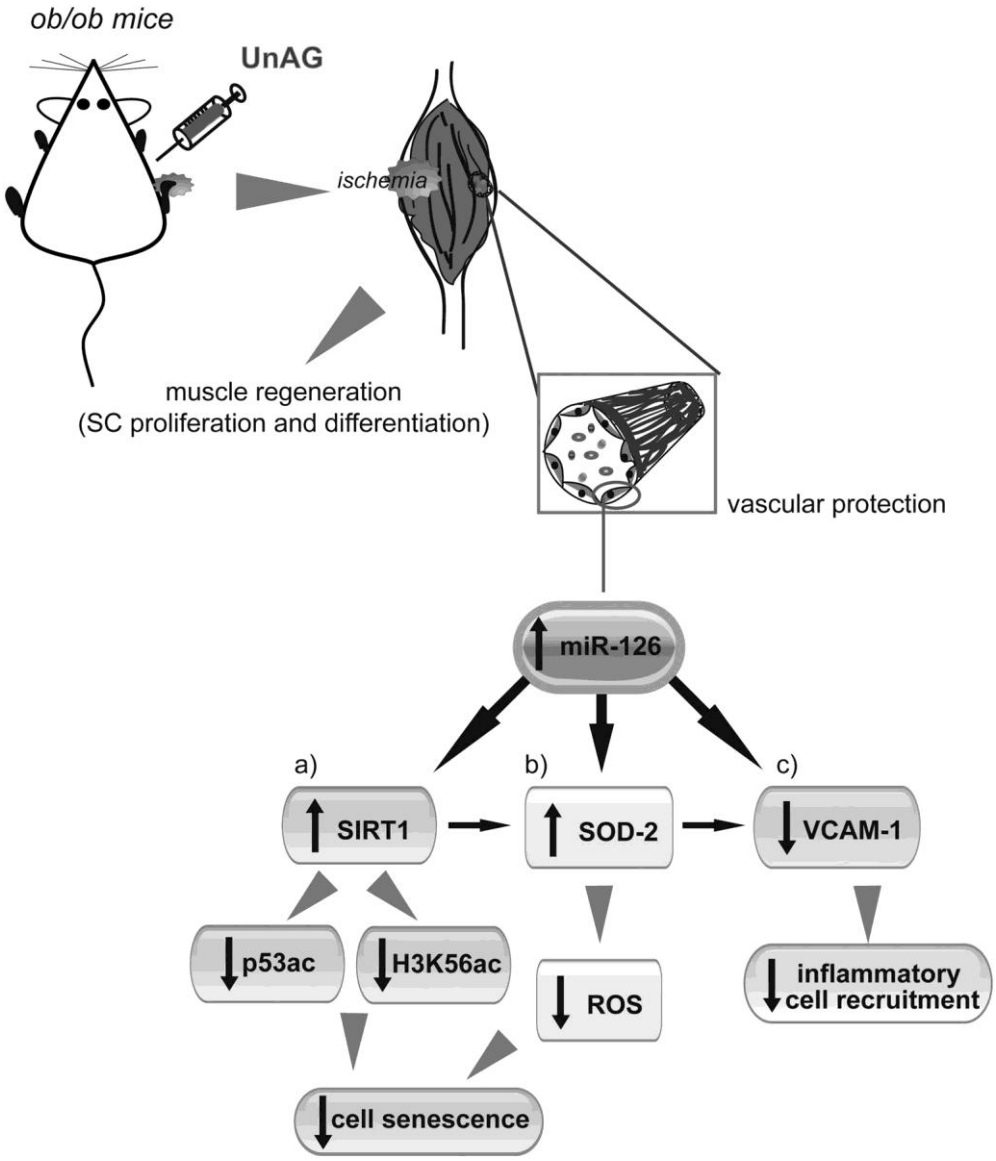
ob/ob mice
UnAG
ischemia
muscle regeneration
(SC proliferation and differentiation)
vascular protection
miR-126
a)
b)
c)
SIRT1
SOD-2
VCAM-1
p53ac
H3K56ac
ROS
inflammatory
cell recruitment
cell senescence

Figure 8

SUPPLEMENTARY DATA

Supplementary Table 1. Reagents and antibodies

Reagents	
Description:	**Purchased from:**
collagenase IA, FCS, FBS, RNase, SDS, PIPES, Triton X-100, Nonidet P-40, NaCl, NaF, $NaOV_4$, $Na_4P_2O_7$, $MgCl_2$, KCl, HCl, Na-azide, Hepes, Tris, EDTA, EGTA, ethanol, aprotinin, pepstatin A PMSF, DTT, leupeptin, penicillin-streptomycin, HEPES, Trichostatin A, DAPI, sucrose, advanced glycation end-products (AGEs), protein A–Sepharose beads	Sigma-Aldrich (St Louis, MO, USA)
Protein molecular weight markers, Acrylammide, polyvinylidene difluoride (PVDF) membranes,	Bio-Rad (Hercules, CA, USA)
Gene Ruler™ DNA ladder mix and Gene Ruler™ DNA ladder plus	Fermentas International Inc (Burlington, Canada)
Nylon mesh cell strainer (100 μm, 70 μm, 40 μm)	BD Bioscience Pharmingen (Franklin Lakes, NJ, USA)
UnAG	Phoenix Pharmaceuticals (Belmont, CA, USA)
Lipofectin® Reagent, TRIzol, DMEM Amplex Red Assay kit	Invitrogen™ (Life Technologies Carlsbad, CA, USA; Paisley, UK).
Nitric oxide assay kit	Abcam (Cambridge, UK),
Isofluorane	Aerrane®, Baxter , Italy
Antibodies an anti-miR126	
Description:	**Purchased from:**
monoclonal anti-PCNA anti- H3K56ac anti-H3 anti-pS36p66Shc	Abcam (Cambridge, UK)
anti CD31 anti CD68	BD Bioscience Pharmingen (Franklin Lakes, NJ, USA)
anti SIRT1 Cyclin D1 anti SOD-2 anti VCAM-1 anti-p53 anti-p66 shc Pax-7 MyoD myogenin	S. Cruz Biotechnology (Heidelberg, Germany)
anti-pAMPK anti-AMPK anti-acetylated-Lys382 p53 antibody	Cell Signaling (Danver, MA, Usa).
anti rabbit IgG, HRP linked anti mouse IgG, HRP linked	Southern Biotech (Birmingham, AL 35209, USA)
anti mouse, rabbit and goat IgG-TRITC anti mouse, rabbit and goat IgG-FITC anti-miR-126 antagonist	Life Technologies (Carlsbad, CA, USA; Paisley, UK)
anti β-actin	Sigma-Aldrich (St Louis, MO, USA)

SUPPLEMENTARY DATA

Murine hind limb ischemia model. Male C57BL/6J ob/ob mice (8 weeks-old) (Charles River Laboratories International Inc., Wilmington, MA, USA) were anesthetized on day 0 with isofluorane (2 to 2.5 % in 100 % oxygen) and unilateral hind limb ischemia was induced, as described in (1).
The entire right hind limb femoral artery and vein were exposed and isolated from the inguinal region to the bifurcation of the saphenous/popliteal artery. Exposed vessels were ligated at their proximal and distal ends (poplitea ramification), and both vessels were excised. The normo-perfused contra-lateral limb of each mouse was used as an internal control.
After hind limb ischemia, animals (13 mice per group) were treated daily with an intra-peritoneal injection, from 0 to day 21, that contained either saline or UnAG (100 μg/kg). Mice were treated according to European Guidelines and policies as approved by the University of Turin's Ethical Committee.

Laser Doppler Perfusion Imaging (LDPI). Mice were anesthetized as above and hair was removed using an electric shaver. A serial, non-invasive assessment of ischemic limb micro-vascular perfusion was performed in triplicate and in a blinded manner using the LDPI system (PIM3, Perimed). Identical regions, that were equal in area and that encompassed the distal leg (entire foot) of both ischemic and contralateral, non-ischemic limbs were assessed for perfusion quantification using LDPI processing software (v5.0) (performed at WIL Research Europe Saint Germain-Nuelles, France).

***In vivo* assessment of limb function.** A semiquantitative estimation of foot damage (2-way ANOVA followed by the post-hoc test with Bonferroni correction for multiple comparison) was performed serially using the following classification: 3=dragging of foot (foot necrosis), 2=no dragging but no plantar flexion (foot damage), 1=plantar flexion but no toe flexion (toe damage), and 0=flexing the toes to resist gentle traction on the tail (no damage) (2).

Histological, immunofluorescence and immunohistochemistry analysis. Gastrocnemius muscles were recovered from the ischemic and normo-perfused limbs of treated animals, fixed in 10% formalin and embedded in paraffin. Tissue sections (5 μm) were stained with hematoxylin and eosin for histological analysis. The proportion of fibers with central nuclei (regenerating fibers) was counted in the injured area and the cross-sectional areas of the fibers in the injured and non-injured areas. Measurements were obtained using the MetaMorph software (Life Sciences Research Imaging Systems). Muscle sections were processed for immunofluorescence assays as previously described (3) using anti-CD68, anti-SOD-2, anti-CD31 and anti-SIRT1 antibodies. DAPI was used as a nuclear marker. In order to quantify cells that express the indicated markers, positive cells were counted in 10 randomly selected fields in 5 different samples (40X magnification). The number of CD31-positive vessels was evaluated by counting 10 randomly selected fields in 3 different samples (40X magnification). Images were acquired using a Zeiss LSM 5 Pascal confocal laser-scanning microscope (Carl Zeiss, Jena, Germany) which was equipped with a helium/neon laser (543 mm), an argon laser (450-530 mm) and an EC planar Neofluar 40×/1.3 oil-immersion differential interference contrast objective lens. Images were analyzed using Zeiss LSM 5 version 3.2 software (4).
For immunohistochemistry analysis, sections from paraffin-embedded samples were collected and placed onto poly-lysine–coated slides. Endogenous peroxidase activity was blocked with 6% H_2O_2 for 8 minutes at room temperature. The anti-VCAM-1 antibody was applied to slides overnight at 4°C in order to detect VCAM-1 expression. Horseradish peroxidase–labeled anti-rabbit Envision polymer (DakoCytomation, Carpinteria, CA) was incubated for 30 minutes. The reaction product was developed using 3,3-diaminobenzidine. The omission of the primary Ab or substitution with an unrelated rabbit serum IgG served as a negative control. The percentage of positive cells was counted in 4 non-sequential sections for each experiment at 40X magnification (5).

SUPPLEMENTARY DATA

Cell cultures and *in vitro* ischemia. The *ex vivo* experiments saw endothelial cells (ECs) being isolated from gastrocnemius muscles that had been subjected to ischemia (6 mice). Muscles were finely minced with scalpels and digested by incubation for 1h at 37°C in HBSS that contained 0.1% collagenase IA. After washing in the medium plus 10% Bovine Calf Serum (BCS), the cell suspension was then passed through a graduated series of nylon mesh cell strainers (100µm, 70µm and 40µm) which separated mononuclear cells from muscle fibers and myofibril fragments. Cells were re-suspended and ECs were isolated using the anti-mouse CD31 antibody coupled to magnetic beads by magnetic cell sorting using the MACS system (Miltenyi Biotech, Auburn, CA) (6). Briefly, cells were labeled with the anti-mouse CD31 antibody for 20 min and were then washed twice and re-suspended in MACS buffer (PBS without Ca2+ and Mg2+, supplemented with 1% BSA and 5 mM/L EDTA) at the concentration of 0.5×10^6 cells/80 µl. After washing, the cells were separated on a magnetic stainless steel wool column, according to manufacturer's instructions. Positive separated cells correspond to ECs, while negative separated cells were considered to be principally composed of myofibril fragments. For the *in vitro* experiments, ECs were isolated from the human umbilical vein by Trypsin treatment within 4 hours of delivery (0.1%, w/v), cultured in Medium 199 with the addition of 20% (v/v) BCS and 5 ng/ml of bFGF and used at early passages (II-III). Throughout the study, ECs were cultured for 2 days in normal medium (5 mmol/l D-glucose) plus 10% (v/v) BCS and bFGF (5 ng/ml), either alone or in combination with 400 µg/ml AGE or 25 mmol/l D-glucose (HG) and treated in two groups; either with or without UnAG (1µmol/L). At day 3, cells were subjected to *in vitro* ischemia which was induced by incubating cells in DMEM + 2% Foetal Calf Serum (FCS) at 5% CO_2/95% N_2 humidified atmosphere, yielding 1% O_2 concentrations for 24h (3). SCs were also isolated from the gastrocnemius muscles of ob/ob mice that had been subjected to ischemia, muscle samples were subjected to enzymatic digestion as described (7) to obtain SCs.

Cell proliferation. Cell proliferation of ECs that had been recovered from the ischemic muscles of saline and UnAG-treated mice was assayed by evaluating the percentage of PCNA-positive cells by FACS analysis, as described previously (8). Cyclin D1 expression was evaluated by western blot as previously described (9).

FACS analysis. ECs which had either been treated with the indicated stimuli or had been left untreated were either labeled with the anti-VCAM-1 antibody or with a preimmune monoclonal antibody for 30 minutes at 4°C. They were washed twice in PBS and incubated with fluorescein-labeled anti–mouse IgG for the same amount of time. The expression of cell surface molecules was evaluated by flow cytometry (FACScan; Becton Dickinson, San Jose, CA).

ROS detection. ROS production was performed using the horseradish peroxidase-linked Amplex Red fluorescence assay kit (Molecular Probes, Invitrogen). To this end, Amplex Red (50 µM) and horseradish peroxidase type II (0,1 U/ml) were added to cell lysates and processed according to manufacturer's instructions. All experiments were performed in triplicate (10).

Detection of nitric oxide: NO detection was evaluated by measuring NO production on ECs treated with the indicated stimuli and subjected to *in vitro* ischemia (11). Briefly, equal amounts of proteins were collected and nitrate plus nitrite levels were measured with the Griess assay kit according to manufacturer's instructions (Abcam, Cambridge, UK).

SUPPLEMENTARY DATA

Western blot analysis and nuclear extracts. Cells were lysed (50 mmol/L Tris HCl [pH 8.3], 1% Triton X-100, 10 mmol/L PMSF, 100 U/ml aprotinin, 10 μmol/L leupeptin) and protein concentrations were obtained as previously described (12). Proteins (50 μg) were subjected to SDS-PAGE, transferred onto nitrocellulose membranes, blotted with the indicated antibodies and revealed using a chemiluminescence detection system (ECL). Densitometric analysis was used to calculate the differences in the fold induction of protein levels and normalized to β-actin, H3, p66Shc, AMPK or p53 content. Values are reported as relative amounts. In order to evaluate H3 acetylation, nuclear extracts from ECs, treated with the indicated stimuli and subjected to *in vitro* ischemia, were obtained as previously described (12) and processed as indicated.

p53 acetylation. Cells were lysed in cold DIM buffer (50 mmol/l Pipes, pH 6.8, 100 mmol/l NaCl, 5 mmol/l $MgCl_2$, 300 mmol/l sucrose, 5 mmol/l EGTA, 2 mmol/l sodium orthovanadate plus 1% Triton X-100 and a mixture of protease inhibitors/1 mmol/l phenylmethylsulfonyl fluoride, 10 mg/ml leupeptin, 0.15 U/ml aprotinin and 1 mg/ml pepstatin A) and supplemented with 10 μM Trichostatin A (TSA) to prevent deacetylation after cell lysis. Equal amounts of proteins (500 μg) were immunoprecipitated with p53 monoclonal antibody for 6 h at 4°C and the immunocomplexes were bound to protein A–Sepharose beads at 4°C over night. Bound proteins were eluted and processed as described previously (13). Immunoprecipitates were subjected to SDS-PAGE, transferred onto nitrocellulose membranes, blotted with the anti-acetylated-Lys382 p53 antibody and revealed using a chemiluminescence detection system (ECL). Densitometric analysis was used to calculate the differences in the fold induction of protein levels and normalized to p53 content. Values are reported as relative amounts.

Senescence assay. Senescence was evaluated by measuring acidic β-gal activity on ECs treated with the indicated stimuli and subjected to *in vitro* ischemia, and on ECs recovered from the ischemic muscles of treated animals (14). Briefly, ECs were washed in PBS, fixed for 3 minutes at room temperature in 2% paraformaldehyde, washed and incubated for 24 hours at 37°C with fresh SA-β-gal stain solution: 1 mg/ml 5-bromo-4-chloro-3-indolyl β-D-galactopyranoside (X-gal), 5 mM potassium ferrocyanide, 5 mM ferricyanide, 150 mM NaCl, 2 mM $MgCl_2$, 0.01% sodium deoxycholate and 0.02% Nonidet P-40. Senescence was expressed as the percentage of SA-β-gal-positive cells over a total of 100 cells, manual count at 20X magnification by 3 independent investigators.

Silencing of the endogenous SIRT1 and SOD-2 by small interfering RNAs (siRNAs) In order to obtain SIRT1 and SOD-2 inactivation, ECs were transiently transfected with siRNA for SIRT1, with siRNA for SOD-2 or with duplex siRNAs (Qiagen, Valencia, CA, USA) (13) and treated as indicated. Transfection was performed according to manufacturer's instructions. Whole cell extracts were processed 48h after transfection. Cell viability was evaluated at the end of each experiment

Adhesion assay. The adhesion of peripheral blood mononuclear cells (PB-MNCs) on ECs that had either been silenced for SIRT1, SOD-2 or miR-126 or not, and treated as indicated, was assayed. Briefly, PB-MNCs, obtained by Ficoll Histopaque 1077 (Sigma-Aldrich) were labeled with the red fluorescent PKH26 (Sigma-Aldrich) vital dye and, after centrifugation at 1400*g* for 10 minutes, re-suspended in medium free that contained 0.25% bovine serum albumin. Cells were then added (at 2×10^5 cells per well) to a confluent monolayer of ECs, that had either been left untreated or treated as indicated. Co-cultures were thus incubated at 37°C for 4h and non-adherent cells were removed by being washed three times with a phosphate-buffered saline. Samples were then fixed with 4% formaldehyde/phosphate-buffered saline and observed under an epifluorescence microscope. Bound labeled cells were counted by three different operators in triplicate (10 fields at × 20 magnification per sample).

SUPPLEMENTARY DATA

RNA isolation and quantitative real-time PCR (qRT-PCR) for miRNAs. Total RNA was isolated using the TRIzol reagent (Invitrogen), either from ECs that had been recovered from the muscles of treated animals or from ECs that had been subjected to *in vitro* ischemia. The RNA was then reverse-transcribed using a TaqMan microRNA RT kit, specific for miR-126, and subjected to qRT-PCR using a TaqMan microRNA assay kit and the ABI PRISM 7700 sequence detection system (Applied Biosystems). miRNA expression was normalized to the small nuclear RNA RNU6B. Loss-of-function experiments were performed in saline- or UnAG-treated ECs that had been transfected for 48 h with the anti-miRNA negative control or the anti-miR-126 antagonist (Applied Biosystem, Foxter Cyto CA, USA), according to manufacturer's instructions (6).

Luciferase gene reporter. The luciferase reporter assay was performed using a construct generated by subcloning the PCR products amplified from the full-length 3'UTR of VCAM-1 DNA into the xbaI restriction site of the luciferase reporter vector pGL3 (Promega Italia S.R.L., Milano Italy). The PCR products were obtained using the following primer: VCAM-1: 3' UTR response element: GTATAGTACTGGCATGGTACGG. The insert identities were verified by sequencing. The pGL3, pGL3-3'UTR VCAM-1 reporter vectors were transiently co-transfected in ECs that had been subjected to *in vitro* ischemia and treated, as indicated, at a 10:1 molar ratio with the pRL vector, that codes for *Renilla* luciferase, used as an internal control for the luciferase assay (15).

Blood glucose measurement. Just before sacrifice, the maximum volume of blood from each group of mice was collected under isofluorane anaesthesia (Aerrane®, Baxter) from the abdominal aorta. Recovered plasma glucose levels (Charles River Lab, Lecco, Italy) are reported: 7 saline-treated ob/ob mice (blood glucose, 326.3 ± 28.9 mg/dL); 7 UnAG-treated mice (blood glucose, 310.1 ±31.2 mg/dL). Blood glucose was measured using a One Touch II glucose meter (Lifescane, Mountain View, CA), according to manufacturer's instructions. Glycated hemoglobin was measured in whole blood samples by quantitative immunoturbidimetric latex determination (Sentinel Diagnostic, Milan, Italy).

Glucose Tolerance (GTT) and Insulin Tolerance Tests (ITT). Glucose tolerance and insulin sensitivity, evaluated in 8 week old ob/ob mice (6 mice), were measured as follows: mice were subjected to 16 hrs of fasting and injected i.p. with 1 g glucose/kg body weight (20% D-glucose, Sigma, in 0.9% saline) for GTT, and 0.75 U insulin/kg body weight (Humulin R, Lily, Indianapolis, USA) for ITT, as indicated. Glucose levels [mg/dL] (tail blood) were measured using a One Touch II glucose meter (Lifescane, Mountain View, CA), before (0 min) and at time intervals (30, 60, 90 and 120 min) after injection. (16).

Statistical analysis. All data are presented as mean±SEM. The D'Agostino–Pearson test was used to test normality. Data on blood perfusion, damage score, number of vessels, percentage of regenerating fibers, inflammatory cells, miR-126 and VCAM-1 expression from the ischemic and non-ischemic limbs of treated ob/ob mice at days 7 and 21 were analyzed using 2-way ANOVA, followed by the *post-hoc* test with the Bonferroni correction for multiple comparisons. Data on blood glucose, body weight, HbA1c measurements, from adhesion assays, senescence assays, on ROS generation, NO production, CD31/SOD-2 co-localization, CD31/SIRT1 co-localization, PCNA expression, on GTT or ITT assay, from luciferase assays, on miR-126 expression in *in vitro* or in loss-of-function experiments and SIRT1 and SOD-2 inactivation were analyzed using 1-way ANOVA followed by Tukey's multicomparison *post-hoc* test. Densitometric analysis data for the Western blots were analyzed using Student *t* tests for 2-group comparison and using 1-way ANOVA, followed by Tukey's multiple comparison test, for ≥3 groups. The cut-off for statistical significance was set up at $P<0.05$ (*$P<0.05$, **$P<0.01$, ***$P<0.001$). All statistical analyses were carried out using GraphPad Prism version 5.04 (Graph Pad Software, Inc).

REFERENCES

1. Hellingman AA, Bastiaansen AJ, de Vries MR, Seghers L, Lijkwan MA, Löwik CW, Hamming JF, Quax PH. Variations in surgical procedures for hind limb ischaemia mouse models result in differences in collateral formation. Eur J Vasc Endovasc Surg 2010;40:796-803
2. Bosch-Marce M, Okuyama H, Wesley JB, Sarkar K, Kimura H, Liu YV, Zhang H, Strazza M, Rey S, Savino L, Zhou YF, McDonald KR, Na Y, Vandiver S, Rabi A, Shaked Y, Kerbel R, Lavallee T, Semenza GL. Effects of aging and hypoxia-inducible factor-1 activity on angiogenic cell mobilization and recovery of perfusion after limb ischemia. Circ Res 2007;101:1310-1318
3. Togliatto G, Trombetta A, Dentelli P, Cotogni P, Rosso A, Tschöp MH, Granata R, Ghigo E, Brizzi MF. Unacylated ghrelin promotes skeletal muscle regeneration following hindlimb ischemia via SOD-2-mediated miR-221/222 expression. J Am Heart Assoc 2013;2:e000376
4. Zeoli A, Dentelli P, Rosso A, Togliatto G, Trombetta A, Damiano L, di Celle PF, Pegoraro L, Altruda F, Brizzi MF. Interleukin-3 promotes expansion of hemopoietic-derived CD45+ angiogenic cells and their arterial commitment via STAT5 activation. Blood 2008;112:350-361
5. Brizzi MF, Dentelli P, Rosso A, Calvi C, Gambino R, Cassader M, Salvidio G, Deferrari G, Camussi G, Pegoraro L, Pagano G, Cavallo-Perin P. RAGE- and TGF-beta receptor-mediated signals converge on STAT5 and p21waf to control cell-cycle progression of mesangial cells: a possible role in the development and progression of diabetic nephropathy. FASEB J. 2004;18:1249-1251
6. Togliatto G, Trombetta A, Dentelli P, Rosso A, Brizzi MF. MIR221/MIR222-driven post-transcriptional regulation of P27KIP1 and P57KIP2 is crucial for high-glucose- and AGE-mediated vascular cell damage. Diabetologia 2011;54:1930-1940
7. Musarò A, Barberi L. Isolation and culture of mouse satellite cells. Methods Mol Biol 2010;633:101-111
8. Dentelli P, Rosso A, Olgasi C, Camussi G, Brizzi MF. IL-3 is a novel target to interfere with tumor vasculature. Oncogene 2011;30:4930-4940
9. Brizzi MF, Dentelli P, Pavan M, Rosso A, Gambino R, Grazia De Cesaris M, Garbarino G, Camussi G, Pagano G, Pegoraro L. Diabetic LDL inhibits cell-cycle progression via STAT5B and p21(waf). J Clin Invest 2002;109(1):111-119
10. Zgheel F, Alhosin M, Rashid S, Burban M, Auger C, Schini-Kerth VB. Redox-Sensitive Induction of Src/PI3-kinase/Akt and MAPKs Pathways Activate eNOS in Response to EPA:DHA 6:1. PLoS One 2014;9:e105102
11. Dhar A, Dhar I, Desai KM, Wu L. Methylglyoxal scavengers attenuate endothelial dysfunction induced by methylglyoxal and high concentrations of glucose. Br J Pharmacol 2010;161:1843-1856
12. Dentelli P, Trombetta A, Togliatto G, Zeoli A, Rosso A, Uberti B, Orso F, Taverna D, Pegoraro L, Brizzi MF. Formation of STAT5/PPARgamma transcriptional complex modulates angiogenic cell bioavailability in diabetes. Arterioscler Thromb Vasc Biol 2009;29:114-120
13. Uberti B, Dentelli P, Rosso A, Defilippi P, Brizzi MF. Inhibition of β1 integrin and IL-3Rβ common subunit interaction hinders tumour angiogenesis. Oncogene 2010;29:6581-6590
14. Togliatto G, Trombetta A, Dentelli P, Baragli A, Rosso A, Granata R, Ghigo D, Pegoraro L, Ghigo E, Brizzi MF. Unacylated ghrelin rescues endothelial progenitor cell function in individuals with type 2 diabetes. Diabetes 2010;59:1016-1025

15. Harris TA, Yamakuchi M, Ferlito M, Mendell JT, Lowenstein CJ. MicroRNA-126 regulates endothelial expression of vascular cell adhesion molecule 1. Proc Natl Acad Sci U S A 2008;105:1516-1521
16. Kirchner H, Heppner KM, Holland J, Kabra D, Tschöp MH, Pfluger PT. Ablation of ghrelin O-acyltransferase does not improve glucose intolerance or body adiposity in mice on a leptin-deficient ob/ob background. PLoS One 2013;8:e61822